Dissipation rate estimation in a rectangular shaped test section with periodic structure at the walls.

Nicolas La Forgia[a,*], Eirik Helno Herø[a], Jannike Solsvik[a], Hugo Atle Jakobsen[a]

[a]*Department of Chemical Engineering, Norwegian University of Science and Technology (NTNU), Trondheim, Norway*

Abstract

An experimental study of turbulent flow concerning the characterization of turbulence by two-point correlation and estimations of the turbulent dissipation rate is presented. The fluid used is deionized water and the test section used was a square shaped channel of $24mm$ by $30mm$ on the cross section with a length of $1m$. The test section also presented periodic baffle structure at two of the walls for enhancing and maintaining turbulence. The study consisted in the measurement of the velocities at different positions of the channel using Laser Doppler Velocimetry instrument (LDV), the velocity measurement obtained were used for estimating two point correlations using the Taylor's frozen hypothesis. Finally, the results from the two-point correlation were used for estimating the turbulent dissipation rate. Considering the difference in the methods for calculating the dissipation rate, a comparison of the accuracy of each method is presented. It was found that the methods presented in this work showed similar results and trends of the dissipation rate with respect to changes in flow condition and distance to the channel walls. However, better accuracy was obtained by estimating the dissipation rate using the second order structure function and the Kolmogorov's two-third law.

Keywords: Droplet breakage, Experimental investigation, Turbulence measurement, Dissipation Rate

1. Introduction

Turbulence flow are present in many industrial processes, and have become a key parameter in the study of phase interaction in multiphase flows. One particular case of importance for the oil industry is the study of breakage and coalescence of oil droplets in turbulent water. In this case, models for droplets breakage and coalescence are used for the design and modeling of separation processes. While these models concentrate in the evolution of the different phases in the mixture, one key parameter is related to the characterization of the turbulence. Nevertheless, due to the stochastic behavior of the turbulent phenomena the interaction between phases can be difficult to model. As a consequence, most models are based on the statistical probability measured through larger amounts of individual measurement.

A review of droplet breakage mechanisms in static mixer can be found in the work of Lemenand et. al. [1], where shear, elongation and turbulent fluctuation mechanisms are discussed and compared. One important contribution to the modelling of dispersed phase distribution in multiphase flow was presented by Coulaloglou and Tavlarides work [2], in which the foundation for models of droplet breakage and coalescence in turbulent flow for use with Population Balance Equation (PBE) was established. The phenomenological model was derived from a theoretical perspective and validated with the available experimental data where the breakage frequency and coalescence frequency were related to an estimated turbulent dissipation rate. While the model proposed presented good agreement with experimental observations, the authors also

*Corresponding author.

Email addresses: nicolas.la-forgia@ntnu.no (Nicolas La Forgia), eirik.h.hero@ntnu.no (Eirik Helno Herø), jannike.solsvik@ntnu.no (Jannike Solsvik), hugo.a.jakobsen@ntnu.no (Hugo Atle Jakobsen)

concluded that in order to improve the model more measurements with uniform turbulent condition and where coalescence and breakage could be observed independently were needed. Following the same principle, Azizi et. al. [3] investigated breakage in a mixer where the volume-average dissipation rate was estimated from measurement of pressure drop in combination with a model for describing the spatial variation of dissipation rate. More recently, models for drop breakage derived in term of the turbulence energy spectrum has been proposed. Han et. al. [4] suggested that the breakage frequency is parent drop size dependant, and thus influenced by the entire energy spectrum distribution using the energy spectrum models proposed by Pope [5] and by Hinze [6]. The authors found a good agreement between their model predictions and the experimental data of Andersson and Andersson [7] and Maaß and Kraume [8]. Solsvik and Jakobsen [9, 10] proposed a model for the second order structure function based on Pope's energy spectrum model which allowed the evaluation of the breakage and coalescence for the entire energy spectrum range. More recent, Gong et. al. [11] proposed a model for studying the coalescence of droplet in turbulent flow by considering the contribution of multiscale turbulent eddies. The structure function model for turbulence were compared with data from direct numerical simulation and with previous models, where the authors claim to have obtained a better accuracy in representing the second order structure function compared to the model of Han et. al. [4] and Solsvik and Jakobsen [9, 10]. Nevertheless, none of these models were compared with experimental measurement.

While different approaches are available for relating the turbulent phenomena to breakage and coalescence in multiphase flows, there is still lack of accurate experimental data regarding the turbulence characteristics and, as a result, models for turbulence had been used instead. In addition, these models require input of turbulent parameters such as the dissipation rate and the turbulent kinetic energy. However, the turbulent dissipation rate, kinetic energy and energy spectrum are not variables that can be directly measured, and must be experimentally determined which in most cases result in determining two-point correlation from the velocity fluctuation [5, 12]. These correlations require measurement of the velocity fluctuation at two points while varying the distance between them. This procedure requires the use of multiple instruments, however, simplification can be made by adopting the Taylor's frozen hypothesis [13] for constructing two-point correlation based on measurements from a single point.

While the amount of experimental data available in the literature is low, the focus is on models of breakage and coalescence with less focus on the turbulent characterization. Bouaifi et. al. [14] used PIV measurements and CFD simulations using the commercial software Fluent. They compared the commercial software predictions for the axial velocity component with the velocity measured with the PIV and concluded that the low-Reynolds number $k - \epsilon$ turbulence model presented a good agreement with the experiments. Nevertheless, this comparison would only reveal the ability of the model to reproduce the velocity field and not the velocity fluctuation that are required for the turbulence characterization. This work was continued by Andersson et. al. [15] where measurements and simulations of breakage and coalescence were investigated. Here the authors used the PIV technique for obtaining the turbulent kinetic energy and the turbulent dissipation rate which were obtained by direct calculation through the velocity gradients obtained by the PIV method, however the accuracy of the results were not presented. Andersson and Andersson [16] investigated and discussed breakup mechanisms and the dynamics of fluid particle deformation by means of high speed camera and using CFD simulations and PIV method for characterizing the turbulence. Andersson and Andersson [7] proposed a model for fluid particle breakage using the dissipation rate estimated by CFD simulations. Maaß et. al. [17] used the commercial software STAR-CD for estimating the local dissipation rate in a stirred tank for studying breakage phenomena. The model used was based on a $k - \epsilon$ model which showed better prediction at higher flow velocities. Maaß et. al. [18] used the Population Balance Equation (PBE) for investigating the prediction of drop size in stirred tanks. In the PBE model, the authors used the agitation power to calculate the power number accounting the average turbulence dissipation rate. Maaß et. al [19] studied the prediction of droplet size distribution in breakage dominated stirred systems by hindering the coalescence phenomena. In this case, the dissipation rate was calculated by CFD simulations. Maaß and Kraume [8], performed experimental investigations of single drop breakage where the dissipation rate were calculated as in Maaß et. al. [17]. Håkansson et. al. [20], performed experimental investigation to estimate local fragmenting stresses in rotor-stator mixer using two different approach based on PIV measurements. While both methods can provide valuable information, both approaches presented disadvantages related with

the low resolution of the PIV method. Mortensen et. al [21], experimentaly study the effects of slot width on the local dissipation rate of turbulent kinetic energy using a PIV method coupled with a sub-resolution modelling for studying breakage phenomena in roto-stator mixer.

Very few works acknowledged the importance and difficulties in estimating the turbulence parameters. In the work of de Jong et. al. [22], seven different methods for estimating the dissipation rate has been compared using a PIV instrument for the characterization. The uncorrected results obtained using second and third order structure function and the scaling argument presented similar results. However, the uncorrected results obtained using the direct method (measuring the velocity derivatives from the PIV experiments) and the large-eddy PIV method developed by Sheng et. al. [23] results in larger values. The results obtained from the spectral fitting resulted larger values that the second and third structure function methods and the scaling argument but the values were lower than the direct and large-eddy PIV methods. The large-eddy PIV is similar to the direct method but employs the Smagorinsky model [24] for estimating the subgrid stress T_{ij}. In particular, these two methods require a good approximation of the velocity derivatives which can be affected by the spatial resolution of the PIV method. The results were corrected using models obtained from literature that allowed a reduction in the gap between different methods. The corrections diminished the values obtained by the direct method and large-eddy PIV and increased slightly the values from the second and third order structure function method and the scaling argument. Vejrażka et. al. [25] performed experimental measurement of the breakage of air bubbles in a turbulent water flow. The turbulent flow was characterized through the use of the dissipation rate by measuring the velocity field by a PIV system. The local dissipation rate was estimated using a large-eddy PIV technique, a second order structure function method and a scaling argument. The results from the measurement of the dissipation rate from the different techniques presented similar trends with the variation of the flow rate and distances, nevertheless there was a large discrepancy in the values obtained, in which the second order structure function presented systematically lower values for the dissipation rate followed by the large-eddy PIV and finally by the scaling argument.

Lemenand et. al. [26], performed experimental investigation of micro-mixing by chemical probe in homogeneous and isotropic turbulence. The turbulent characteristic was generated by means of an oscillating grid, where the dissipation rate was estimated using a scaling argument based on a three axis LDV measurements. The authors compared the dissipation rate obtained with two different models, showing that the scaling argument used underestimate the dissipation rate compared to the models used. They conclude that the constant of the scaling argument could be greater. In the work of Lemenand et. al. [27], the turbulent dissipation rate was obtained by linear fitting of the energy spectrum model for the inertial sub-range of Kolmogorov [28] using a reconstruction of the energy spectrum based on LDV measurements.

In this paper, measurement of different statistical parameter for characterizing the turbulence in a square channel is presented. It is focused on providing accurate measurements for characterizing the evolution of the turbulence in the channel under different flow conditions. Different parameters were studied; including the turbulent dissipation rate, the second order structure function, third order structure function and the longitudinal autocorrelation function. Several methods are available for estimating dissipation rate from these correlations. These methods will be presented and compared considering the method accuracy and the statistical error in each case.

The design of the experimental apparatus used in this work were previously presented in Shi et. al [29], where the design of the wall structures for the turbulence enhancing were investigated using Large Eddy Simulation method using the commercial software Fluent. The experimental apparatus was designed to study the breakage probability of oil droplet in turbulent flow. More recent, measurement for fully developed turbulent flow were presented and compared with the results from the simulations [30]. The results from the simulations and the dissipation rate estimated from the measurements presented a good agreement. Nevertheless, the injection of oil droplet in a fully developed turbulent flow is difficlut to achieve with this design, as a consequence the turbulence needed to be characterized for the entire channel in order to account the evolution of the turbulent flow around the channel inlet.

2. Turbulent flow characterization

Turbulent flow are characterized by the fluctuating behavior of the velocity field. This means that prediction of the flow condition at any time becomes a difficult task. The use of time average or ensemble average operators over the velocity field can provide information on the magnitude and energy of the turbulence fluctuations which can be used for constructing two-points correlations and for estimating turbulent dissipation rate [5, 12]. Here, the velocity of a particular spatial point can be separated in a mean velocity component and a fluctuation component:

$$U(\bar{x},t) = \bar{U}(\bar{x}) + U'(\bar{x},t) \tag{1}$$

Where $U(\bar{x},t)$ is the instantaneous velocity, $\bar{U}(\bar{x})$ is a time average mean velocity and $U'(\bar{x},t)$ is the velocity fluctuation.

The evolution of turbulence can be represented by correlating the velocity fluctuations at two different spatial positions. The correlation between spatial positions is stronger when the position is close and tends to vanish as the distance between points increases. This dependence on the position can be used in estimating the turbulent dissipation rate. The calculation of the correlations requieres the simultaneous measurements of the velocities at two different positions. While the measurement at two different positions can be obtained using two instruments, the simultaneous condition can be difficult to achieve. An alternative approach is to use the Taylor's frozen hypothesis [13], which assumes that the turbulent fluctuations of the velocity advect with the fluid. This means that the velocity at a different position in the stream-wise direction can be estimated from the conversion from velocity measurements at one position but differents times. The velocity at the new position can be expressed as:

$$U_x(x+r,t_0) = U_x(x, t_0 - r/\bar{U_x}) \tag{2}$$

Where U_x is the velocity in the stream-wise direction, x is the position in the stream-wise direction, r is the distance between the two points in the stream-wise direction, t_0 is the initial time, and $r/\bar{U_x}$ corresponds to the time that the flow takes to advect the velocity fluctuation. Different two-point correlations can be used for characterizing the turbulent flow. The longitudinal correlation function is based in the product of the velocities at different positions in the stream-wise direction. An ensemble average is used with the product of the two velocities in order to construct the auto correlation matrix:

$$Q_{ij}(\bar{x},\bar{r},t) =< U_i'(\bar{x},t)U_j'(\bar{x}+\bar{r},t) > \tag{3}$$

If Q_{ij} does not depend on time, then it is said that the turbulence is statistically steady. In addition, if it is independent of the position $\bar{x}$, then it is said that the turbulence is statistically homogeneous. If the flow condition does not change over time, it can be assumed that the flow is statistically steady. Nevertheless, the condition for statistically homogeneous is more difficult to achieve specially at flows with turbulence generated at the walls [5].

It should be noted that at large $\bar{r}$, $Q_{ij}(\bar{x})$ tends to 0. Moreover, when the distance $\bar{r}$ approaches 0, then this result in:

$$Q_{ij}(\bar{x},t) =< U_i'(\bar{x},t)^2 >= U_{i,rms}'^2 \tag{4}$$

With this property, a dimensionless form can be found, which for the particular case of the stream wise direction this leads to the longitudinal auto correlation function:

$$f(r) = Q_{xx}(r)/U_{x,rms}'^2 \tag{5}$$

Where $f(r)$ is the longitudinal auto correlation function. This dimensionless function can be used to estimate the integral length scale:

$$\begin{aligned} l &= \int_0^\infty f(r)dr \\ &= \frac{1}{U_{x,rms}'^2}\int_0^\infty Q_{xx}(r)dr \end{aligned} \tag{6}$$

This parameter gives an estimation of the region in which the velocities are appreciably correlated.

A different approach is to construct the second and third order longitudinal structure function:

$$< [\Delta v(r)]^2 > \quad = \quad < [U'_x(x+r) - U'_x(x)]^2 > \tag{7}$$
$$< [\Delta v(r)]^3 > \quad = \quad < [U'_x(x+r) - U'_x(x)]^3 > \tag{8}$$

In the case of the second order structure function, the correlation approaches 0 when r tends to 0 and start developing until it reach its maximum value $< [\Delta v(r)]^2 > \approx 2U'^2_{x,rms}$. It is normally interpreted as a measure of the cumulative kinetic energy contained in eddies of size r and less [5].

A relation between longitudinal auto correlation and the second order structure function can be given as:

$$< [\Delta v(r)]^2 > = 2u'^2(1 - f(r)) \tag{9}$$

Another approach is to work in the wavenumber space where the energy spectrum can be interpreated as the distribution of energy of the different vortex size, and the energy is transmitted from the larger scales to the smaller scales where the dissipation of energy takes place. Different sub-ranges can be identified; the dissipation sub range, the inertial sub range and the energy containing eddies sub range. Early breakage and coalescence models like Coulaloglou and Tavlarides [2] assumed a particular relation between the interaction of turbulent energy and droplet size by accounting the contribution of the inertial sub range of the energy spectrum. In the inertial sub range, the turbulence can be described in terms of the turbulent dissipation rate by means of the well-known Kolmogorov's two-thirds law [28] and the Kolmogorov's four-fifths law [31], which relates the evolution of second order structure function and the third order structure function to the dissipation rate.

The Kolmogorov's two-third law can be described by:

$$< [\Delta v(r)]^2 > = \beta \epsilon^{2/3} r^{2/3} \tag{10}$$

where $\beta = 2$. And the Kolmogorov's four-fifth law can be expressed as:

$$< [\Delta v(r)]^3 > = -4/5 \epsilon r \tag{11}$$

The model for the energy spectrum of Kolmogorov for the inertial sub range follows:

$$E(\kappa) = C\epsilon^{2/3}\kappa^{-5/3} \tag{12}$$

where κ is the wavenumber $\kappa = 2\pi/r$. By measuring these two-point correlations, the value of the dissipation rate can be obtained.

The dissipation rate follows from calculating the rate works of viscous stress on Navier-Stokes equation for a Newtonian fluid [12]:

$$\dot{W} = \int u_i \left(T_{ij} dS_j\right) = \int \frac{\partial}{\partial x_j} \left(u_i T_{ij}\right) dV \tag{13}$$

where $\dot{W}$ is the rate of work, T_{ij} is the stress tensor, dS is a surface differential and dV is a volume differential. The stress tensor for Newtonian fluids can be defined as:

$$T_{ij} = \rho\nu \left(\frac{\partial u_i}{\partial x_j} + \frac{\partial u_j}{\partial x_i}\right) = 2\rho\nu S_{ij} \tag{14}$$

where S_{ij} is defined as the stress tensor:

$$S_{ij} = \frac{1}{2}\left(\frac{\partial u_i}{\partial x_j} + \frac{\partial u_j}{\partial x_i}\right) \tag{15}$$

here it can be seen that S_{ij} and in consequence T_{ij} are symetric. Eq. 13 can then be decomposed in:

$$\frac{\partial}{\partial x_j}\left[u_i T_{ij}\right] = \left(\frac{\partial T_{ij}}{\partial x_j} u_i + T_{ij}\frac{\partial u_i}{\partial x_j}\right) \tag{16}$$

Where the first term is related with the net work of viscous force ($f_i u_i$), and the second term correspond to the rate of change of internal energy of the fluid. Using this relation, the dissipation rate can be defined as:

$$\epsilon = \frac{T_{ij} S_{ij}}{\rho} = 2\nu S_{ij} S_{ij} \tag{17}$$

The calculation of the dissipation rate through Eq. (17) is called the direct method. Measurement using PIV instruments can provide information on a two-dimensional velocity field from which the velocity derivatives can be extracted in order to apply the direct method. The third velocity field in PIV can be estimated for using this method. Nevertheless, the accurate estimation of the velocity derivatives requires a very fine spatial resolution in order to resolve the turbulent dissipation scales. The large-eddy PIV method developed by Sheng et. al. [23] uses the Smagorinsky model [24] for estimating the unresolved smaller scales through the calculation of the sub grid stress T_{ij} in Eq. (17).

LDV methods provides measurement of velocity in one spatial position, however, by means of the Taylor's frozen hypothesis, information on the velocity in the stream wise direction can be obtained. The estimation of the velocity can be used to obtain the velocity derivative for the stream-wise direction. In order to solve the direct method, assumptions must be used for the remaining unknown velocity derivatives. One common approximation is to assume isotropic flow, from which the equation of the dissipation rate for isotropic flow can be simplified [32]:

$$\epsilon = 2\nu S_{ij} S_{ij} = 15\nu \left(\frac{\partial u_x}{\partial x} \right)^2 \tag{18}$$

nevertheless, the error in estimating the velocity derivative can still be large depending on the spatial resolution for each experiment.

A different approximation is based on a scaling argument where it is assumed the turbulent dissipation rate equals the energy passed down the cascade from largest eddies to smaller eddies, and since viscous dissipation is concentrated at smaller scales this leads to the following approximation:

$$G \approx \epsilon \approx u'^2_{rms} \frac{u'_{rms}}{l} = \frac{u'^3_{rms}}{l} \tag{19}$$

where G is the generation of turbulence, u'^2_{rms} is a measure of the kinetic energy and l/u'_{rms} is a measure of the turnover time of the largest eddies. Then the estimation of the dissipation rate from the scaling argument follows:

$$\epsilon = \frac{A u'^3_{rms}}{l} \tag{20}$$

Where the prefactor A is a constant parameter with value ($A \approx 1$).

As mentioned before, the use of the turbulent dissipation rate in the classical breakage and coalescence models were related to the inertial sub range solely. However, more recent developments on breakage and coalescence modeling include the effects from the entire energy spectrum [4, 9]. In this case, the entire energy spectrum cannot be described only in terms of the turbulent dissipation rate. Several models for energy spectrum have been reviewed in the work of Solsvik and Jakobsen [10]. In particular, Pope [5] proposed an empirical model for the entire energy spectrum:

$$E(\kappa) = C \epsilon^{2/3} \kappa^{-5/3} f_L(\kappa L) f_\eta(\eta \kappa) \tag{21}$$

where f_L and f_η are non-dimensional functions, C is the Kolmogorov's constant ($C = 1.62$), and L is the integral scale defined as:

$$L = \frac{k^{3/2}}{\epsilon} \tag{22}$$

where k is the turbulent kinetic energy:

$$k = \frac{3}{2} u'^2_{rms} \tag{23}$$

The function f_L and f_η follows:

$$f_L(\kappa L) = \left(\frac{\kappa L}{[(\kappa L)^2 + c_L]^{1/2}}\right)^{5/3+p_0} \tag{24}$$

$$f_\eta(\kappa\eta) = e^{-\beta\left([(\kappa\eta)^4 + c_\eta^4]^{1/4} - c_\eta\right)} \tag{25}$$

where ($p_0 = 2$, $\beta = 5.2$), c_L and c_η are positives parameter, and η is the Kolmogorov's micro length scale defined in Tennekes and Lumley [33] as:

$$\eta = \left(\frac{\nu^3}{\epsilon}\right)^{1/4} \tag{26}$$

where ν is the kinematic viscosity. The function f_η concern the micro scale as is related with the fluid viscosity, while the function f_L is related to the energy containing sub range by accounting the turbulent kinetic energy k through the integral length scale L. It should be noted that the energy spectrum proposed by Kolmogorov for the inertial sub range has contribution on the entire energy range in the model proposed by Pope, where it follows that the dissipation rate could be considered as the main parameter affecting the entire energy spectrum.

The estimation of the values for C_L and C_η has been proposed in the work of Solsvik [34], where the parameters are presented as functions of the Kolmogorov's constant C:

$$c_\eta(Re_\lambda, C) = \exp\left(\frac{14.043 - 4.222C}{Re_\lambda^{1.986-0.363C}}\right) - [0.089 + 0.339C] \tag{27}$$

$$c_L(Re_\lambda, C) = \exp\left(-\frac{4.478 + 18.362C}{Re_\lambda^{1.075-0.07C}} - 1.342 + 2.024C\right) - 1.913 + 2.169C \tag{28}$$

where Re_λ is the Taylor-scale Reynolds number which is related with the integral scale Reynolds number Re_L:

$$Re_\lambda = \sqrt{\frac{20}{3}} Re_L^{1/2} \tag{29}$$

$$Re_L = \frac{k^2}{\epsilon\nu} \tag{30}$$

Based on Pope's model, Solsvik and Jakobsen [9] presented an analytical solution for the second order structure function considering the energy spectrum model from Pope in the energy containing range and inertial sub-range, and then extended to the dissipation range by including a semi empirical formula proposed

by Sawford and Hunt [35]:

$$
\begin{aligned}
< [\Delta v(r)]^2 > &= \frac{4}{3}k\left(\frac{r^2}{r_d^2+r^2}\right)^{2/3}(1-[T_1(r)+T_2(T_3(r)T_4(r)-T_5(r))]) \\
T_1(r) &= \frac{2}{[s(r)]^2}F\left(\left(-\frac{1}{3}\right)^{1/2},\left(\frac{3}{2}|\frac{[s(r)^2]}{4}\right)\right) \\
T_2 &= 3^{3/2}\Gamma(2/3) \\
T_3(r) &= 27\times 2^{1/3}[s(r)]^{2/3}\Gamma(2/3) \\
T_4(r) &= \frac{1}{352\pi}F\left(\left(\frac{7}{3}\right)^{11/6},\left(\frac{17}{6}|\frac{[s(r)]^2}{4}\right)\right) \\
T_5(r) &= \frac{2^{2/3}}{2\pi[s(r)]^{2/3}}K_{4/3}(s(r)) \\
s(r) &= \frac{\kappa r}{C_L^{-1/2}\kappa L} \\
c_L &= (C\times 1.262)^3 \\
r_d &= (15C_K)^{3/4}
\end{aligned}
\tag{31}
$$

Where, $C_K = 2$, F is the hypergeometric function, K is the Bessel function, and Γ is the gamma function.

More recently, Gong et. al. [11] proposed an alternative empirical model for the second order structure function for the entire energy spectrum:

$$
< [\Delta v(r)]^2 >= \begin{cases} C_K\left(\frac{r^2}{r^2+r_d^2}\right)(\epsilon r)^{2/3}f_L(\kappa L) & \text{for} \quad r\le L \\ C_K\left(\frac{L^2}{L^2+r_d^2}\right)(\epsilon L)^{2/3}f_L(\kappa L) & \text{for} \quad r> L \end{cases} \tag{32}
$$

where f_L is given by Eq. (24). The parameter c_L was taken from Eq. 28.

In addition, the second order structure function can be obtained by integrating the the energy spectrum model from Pope [5]. The integration follows [12]:

$$
< [\Delta v(r)]^2 >= \frac{4}{3}\int_0^\infty E(\kappa)\left[1-3\frac{\sin(\kappa r)}{(\kappa r)^3}+3\frac{\cos(\kappa r)}{(\kappa r)^2}\right]d\kappa \tag{33}
$$

3. Experimental setup

The experimental setup was developed in order to study the breakage of oil droplets in turbulent water flow. The design presents a baffle structure on the channel walls for enhancing the turbulence generation. The design of these structures was simulated using the Fluent software, where the Large Eddy Simulation model was employed. The details of this numerical simulation can be found in the work of Shi et. al. [29].

The experimental setup is presented in Fig. 1. It is a closed loop circuit using destilled water as continuous phase. The fluid is driven from a reservoir tank by a mechanical pump (model MDL-0670 from SPX Flow Technology), then pass through a flow meter (model SITRANS F M MAG 5000 from Siemens) connected to an acquisition card (NI USB-6221 from national instrument) which has a sampling frequency of $250kHz$. Before reaching the measurement section the flow pass through three sections with different cross-sectional areas. The first section presents the largest area while the third section presents the smallest area. Finally, the flow circulates the test section and is recovered in the reservoir tank.

The test section presents a rectangular cross section were two walls are made with glass and the other two walls presents a periodic squared shaped structure for enhancing and sustain the turbulence. The two walls with glass allows the visualization of the fluid flow and the utilization of the Laser Doppler Velocimetry (LDV) measurement. The cross sectional evolution of the three reduction section before the test section

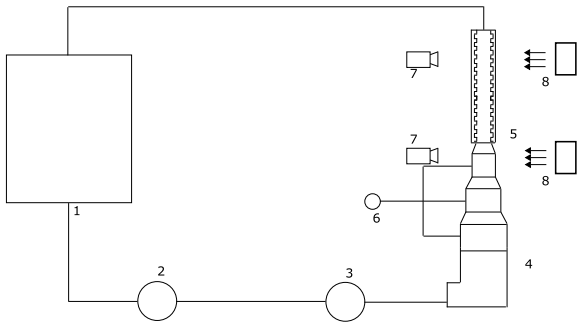

Figure 1: Schematic drawing of experimental setup. 1. Water tank, 2. Pump, 3. Flowmeter, 4. Droplet generation channel, 5. Breakage channel, 6. Syringe pump with oil, 7. Camera, 8. Illumination.

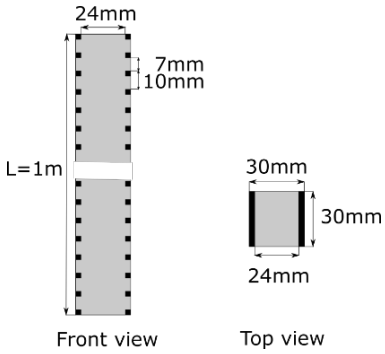

Figure 2: The section view.

help to avoid turbulence before the test section, meaning that turbulence should be generated in the channel walls at the beginning of the test section. In Fig. 2 a view of the test section can be observed along its main dimension, the structures at the wall for creating and enhancing turbulence are presented in black.

The experiments consisted in measurements of the velocity of the fluid at different positions of the channel using a laser Doppler velocimetry (LDV) instrument. Using this technique, the mean value and velocity fluctuation are measured at different points in space. Then the different two-point correlations were calculated. Finally, the dissipation rate was estimated using the different relations presented in the previous section.

In the present paper, oil droplets were not used during the turbulent characterization. However, when experiments involves the use of oil droplets these are separated by gravity in the water reservoir. The volume of water in the reservoir is approximately around 800 to 900 liters, and the amount of oil used during experiments is small which means that the oil can be separated by gravity and collected at the top of the water tank where it is removed manually.

3.1. Laser Doppler Velocimetry

A laser Doppler velocimetry (LDV) model Fiberflow from Dantec Dynamics was used for the measurements. The instrument measures single point velocities by the Doppler Shift of laser beams reflected by seeding particles in the fluid media. With two pairs of laser beams, it was possible to get two velocity directions, stream-wise and normal to the baffled walls. To map a plane in the center between the two glass sides the probe emitting the laser beams was mounted on an automatic traverse system such that it could move stream wise and between the baffled channel sides. In each point, a dataset of velocities was obtained.

3.2. Experimental procedure

The measurement procedure consisted in selecting the flow condition (flow rate). Then, using the measurement from the flow-meter, the pump was adjusted to achieve the targeted condition. Then using two motorized stages, the laser were positioned at different locations of the channel. The positioning of the laser were performed in order to map the entire visible area of the channel. For this reason, a grid of points were constructed and measurements were performed at each point.

The grid of points were constructed using 17 points in the stream axis and 11 points in the perpendicular direction (wall distance). The first point in the stream wise direction was located at 100 mm from the channel entrance and the last point at 900 mm. The points perpendicular to the wall were measured in term of the distance to the wall starting at 0.5 mm of distance and to the middle of the channel at a distance of 12 mm from the wall.

3.3. Instrument error

The flow condition was measured using a flow meter that has an accuracy of 0.4% of the measured flow rate. The measurements of the flow presented also a statistical error which could be related to pump oscillations and instrument fluctuations of $\pm 15\, mm/s$. This value was approximately constant at the different flow conditions, meaning that the relative error in the flow is larger for lower flow rate. Nevertheless, the error of the mean diminishes with the number of sampling, where with a sampling frequency of $250kHz$, the error of the mean results 500 times smaller for the mean value with a sampling period of one second. Finally, considering that the minimum flow rate used corresponded to a mean cross sectional velocity of $1.0\, m/s$, the statistical error can be neglected in comparison with the instrument accuracy.

Using the accuracy in the flow measurements, the error in the measurement of the mean flow follows:

$$\frac{\delta U}{U} \approx 0.004 \tag{34}$$

here U is the mean cross sectional velocity.

The error in the velocity measurements is related with the accuracy of the LDV instrument. Systematics error can be improved with calibration of the LDV instruments [36]. However, since no calibration were done an uncertainty of 10 % will be used for estimating the errors. Nevertheless, the focus of this study is on the velocity fluctuations, and since systematic errors affects the mean value, then it is expected that systematic errors would not affect the measurements of the velocity fluctuation.

$$\frac{\delta u}{u} = 0.1 \tag{35}$$

The error in the estimation of the distance between two measurement points r necessary for estimating two points correlations is related with the fluid velocity at each position and the time interval between particles detected by the LDV system:

$$r = \frac{\Delta t}{u} \tag{36}$$

Where u is the mean velocity at a given position. Considering that the uncertainties from the time measurement and the mean velocity measurement are random and independent, we can apply the square root of sum of squares of relative error for the error propagation of r:

$$\frac{\delta r}{r} = \sqrt{\frac{\delta \Delta t}{\Delta t}^2 + \frac{\delta u}{u}^2} \tag{37}$$

For estimating the error on the time interval, we considered the precision in which the LDV measured time. At the maximum fluid velocities used ($2.5\, m/s$), the maximum frequency for particle detection were approximately 2000 particles per second, which gives on average $0.5\, ms$ between particles. Considering that

the instrument can report time interval with a $1\mu s$ resolution, it was consider this as the instrument error and therefore:

$$\frac{\delta \Delta t}{\Delta t} < \frac{1\mu s}{500\mu s} = 0.002 \tag{38}$$

It should be noted that at lower pumping speed, the time between particles increase and therefore the error in the detection of time interval decreases. The error for r from Eq. 37 results:

$$\frac{\delta r}{r} = 0.1 \tag{39}$$

4. Measurements

The measurements consisted in acquiring the velocity fluctuation for different flow conditions and at different positions in the channel. The flow conditions are expressed in terms of the average cross sectional velocity of the flow. The velocity used were $1.0m/s$, $1.5m/s$, $2.0m/s$ and $2.5m/s$. From the measured instantaneous average velocity at each position, the root mean square of the velocity was computed, which was later used for estimating the dissipation rate. For each position, the amount of samples used for the averaging procedure were $N = 200000$.

4.1. Velocity fluctuation

The velocity fluctuation is a statistical quantity that is computed as an average of many samples. Since the mean value of the velocity fluctuation is zero, then it can be related with the measurement of the standard deviation of the velocity measurement:

$$(u'_{rms})^2 =< u'^2 >= \sigma^2 \tag{40}$$

where σ is the standard deviation of the measurement of the velocity. The error of the estimation of $< u'^2 >$ follows the error estimation of the standard deviation [37]:

$$\delta\sigma = \sigma \frac{1}{\sqrt{2(N-1)}} \tag{41}$$

Where N is the number of samples used in the averaging procedure ($N = 200000$). Using this relation, then the relative error of u'_{rms} follows:

$$\frac{\delta u'_{rms}}{u'_{rms}} = \frac{\delta\sigma}{\sigma} = \frac{1}{\sqrt{2(N-1)}} = 0.0016 \tag{42}$$

In Fig. A.20 in Appendix A, the root mean square of the velocity fluctuations are presented for different flow conditions and positions in the channel. It can be observed that the velocity fluctuations start developing at the walls and increases from the start of the channel until approximately the middle of the channel. Then it appears to be independent with the distance to the channel inlet, and close to the end of the channel (at distance $900mm$), it decreases slightly.

Another source of error in the velocity fluctuations is produced by the abrupt change in the mean velocity profile close to the channel wall. The LDV instrument measures the instantaneous velocities of seeding particles that pass through the laser beam. The seeding particles that are detected in each measurement can be associated to a volume around the measurement point defined by the laser beam size, and since the velocity field close to the wall has large velocity gradient, then the velocity measurement of the LDV will be affected by the large velocity distribution inside the volume of detection, resulting in overestimation of the root mean square of velocity fluctuation. In addition, since the amount of particles detected is correlated with the traveling velocity of these particles, the distribution of velocities may not be homogeneous inside the measuring volume. These two sources of error will be translated in larger estimation of the mean velocity and the velocity fluctuation close to the channel wall, resulting in overestimation of the turbulent dissipation rate estimated by the scaling argument.

4.2. Longitudinal autocorrelation function

The values for the longitudinal autocorrelations function result from the ensemble average over a large set of data. The data obtained is separated according to the distance r calculated using the Taylor's Frozen hypothesis. First, a value for r is calculated according to the time between the velocity measurements. Then with this set of velocity and distances, the distances were grouped into smaller regions in order to obtain an average value. Each group were selected using a distance between points of $\Delta r = 0.5mm$, this value was selected taking into consideration the amount of samples to be averaged in each group and the accuracy in resolving the given direction. On one hand, narrower groups could lead to higher position accuracy at the expense of decreasing in the accuracy of the averaged velocity fluctuation measurement. On the other hand, wider groups provide more samples to increase the accuracy of the averaged velocity fluctuations while the position accuracy decreases.

In Fig. 3, an example of the relation between distance and the autocorrelation function Q_{xx} is shown for different flow conditions and distances to the channel wall. The flow selected corresponds to a fully developed flow situated approximately in the middle of the channel at a distance of $600mm$ from the inlet of the channel. From this measurement, it can be observed that the correlation is larger for those positions closer to the channel wall, and it can be observed that the fluctuation of the correlation is also larger for these cases. This last observation could be related with the abrupt change in the velocity profile close to the channel wall.

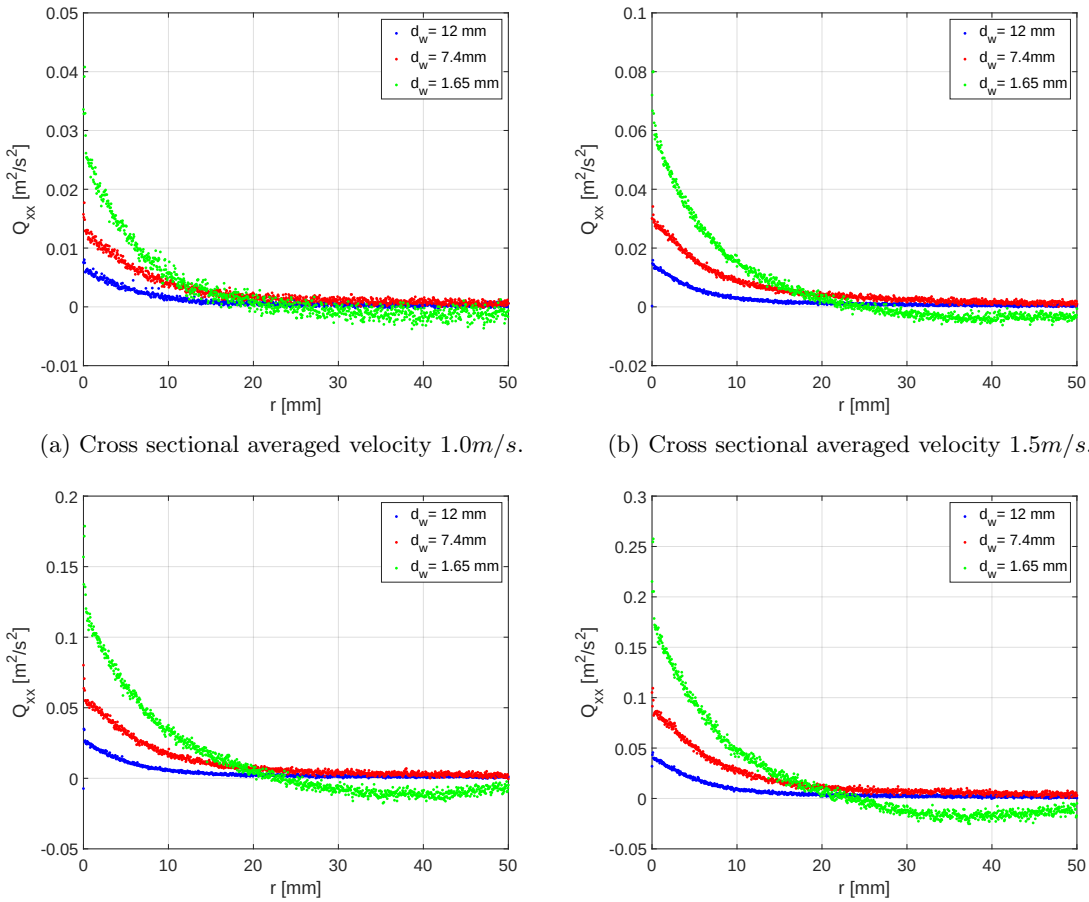

(a) Cross sectional averaged velocity $1.0m/s$.

(b) Cross sectional averaged velocity $1.5m/s$.

(c) Cross sectional averaged velocity $2.0m/s$.

(d) Cross sectional averaged velocity $2.5m/s$.

Figure 3: Velocity correlation function for different flow conditions at $600\,mm$ from the channel inlet. The different measurements correspond to different distances to the channel wall.

The standard deviation of the mean value of Q_{xx} can be estimated as [37]:

$$\delta\bar{Q}_{xx}(r) = \frac{\delta Q_{xx}(r)}{\sqrt{N_r(r)}} \tag{43}$$

Where $\delta\bar{Q}_{xx}$ denotes the error of the mean value, $\delta Q_{xx}(r)$ can be estimated through the standard deviation of the averaging procedure performed in each group of r, and $N_r(r)$ is the number of samples used in the averaging procedure, where different samples number correspond to different values of r.

4.3. Second order structure function measurements

Using the same procedure as for the longitudinal autocorrelation function, an ensemble average of the difference between velocities at two different points in the same stream-wise direction was calculated using a set of data grouped in sections of $\Delta r = 0.5\,mm$. The results for the case with fully develop flow at a distance of $600\,mm$ from the inlet of the channel is shown in Fig. 4. It can be seen that in line with the previous case, the turbulence intensity is larger closer to the channel walls, with larger fluctuation of the correlation for the same case.

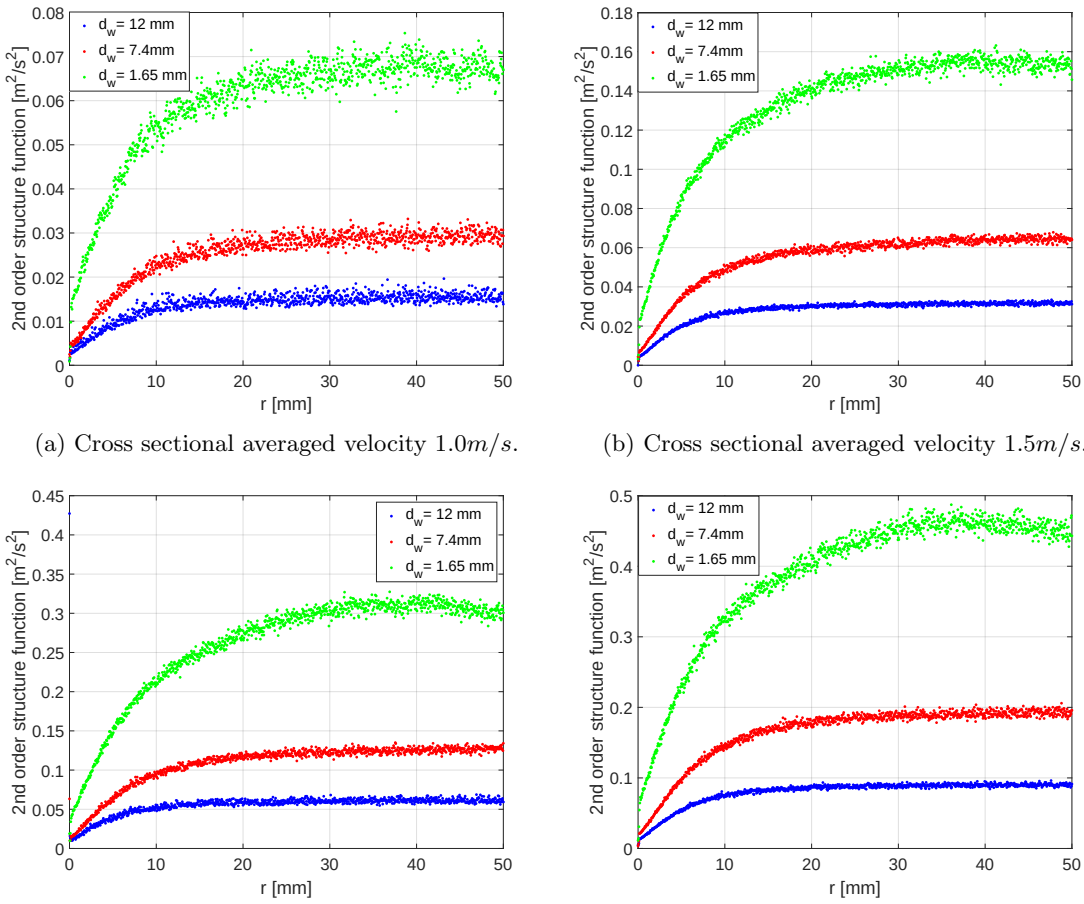

(a) Cross sectional averaged velocity $1.0m/s$.

(b) Cross sectional averaged velocity $1.5m/s$.

(c) Cross sectional averaged velocity $2.0m/s$.

(d) Cross sectional averaged velocity $2.5m/s$.

Figure 4: Second order structure function for different flow conditions at $600\,mm$ from the channel inlet. The different measurements correspond to different distances to the channel wall.

4.4. Third order structure function measurements

The measurement of the third order structure function can be observed in Fig. 5. Here the observed fluctuation in the measured values of the correlation are larger than for the previous two cases, and therefore the expected accuracy that can be obtained from using this correlation should be lower than using the second order structure function measurements. In addition, the data fluctuation that can be observe for low velocities would make it more difficult to perform a curve fitting of the data. Nevertheless, it can be observed that at higher velocities the dependency of the third order structure function with the distance is more clear and in particular closer to the channel wall where it is expected to observe stronger turbulence intensities, showing that the third order structure function can still be a useful tool for the characterization of the turbulence.

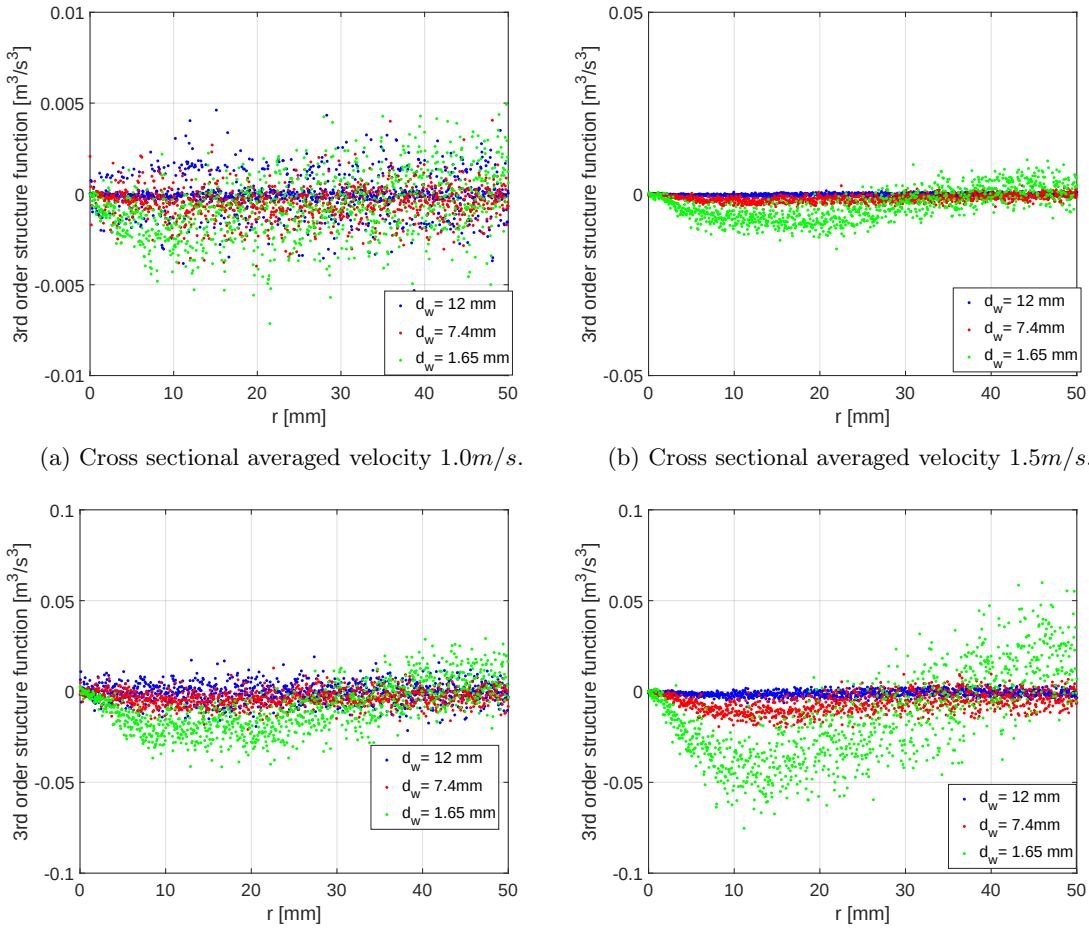

(a) Cross sectional averaged velocity $1.0m/s$.

(b) Cross sectional averaged velocity $1.5m/s$.

(c) Cross sectional averaged velocity $2.0m/s$.

(d) Cross sectional averaged velocity $2.5m/s$.

Figure 5: Third order structure function for different flow conditions at $600\,mm$ from the channel inlet. The different measurements correspond to different positions along the channel length.

5. Integral length scale estimation

The integral length scale has been estimated to be used in Eq. (20) to compute the turbulent dissipation rate. The integral length scale is obtained by integration of the velocity autocorrelation function according to Eq. (7), using the estimation of Q_{xx} and u'_{rms}. The values obtained can be observed in Fig. 6for different

positions of the channel and different flow conditions. It can be observed that the values are in the same range and with very little variation at different velocities or distance to the wall, presenting minimum values close to the channel wall and the middle of the channel. Lower value of the integral length scale close to the channel wall could be due to the presence of smaller turbulent structures. When these structures moves into the flow, they interacts with other structure and as a result, they could increase their size. This could explains why the integral length scale measurements shows first an increase with the distance to the channel wall. The decrease of the integral length scale close to the middle of the channel could be related with the loss of energy due to dissipation. In addition, entrance effects affect the integral length scale estimation in the middle of the channel, since the turbulence levels are smaller in the middle of the channel close to the entrance of the test section. This last hypothesis is sustained by the fact that this effect is observed greater for the channel position closer to the entrance of the test section.

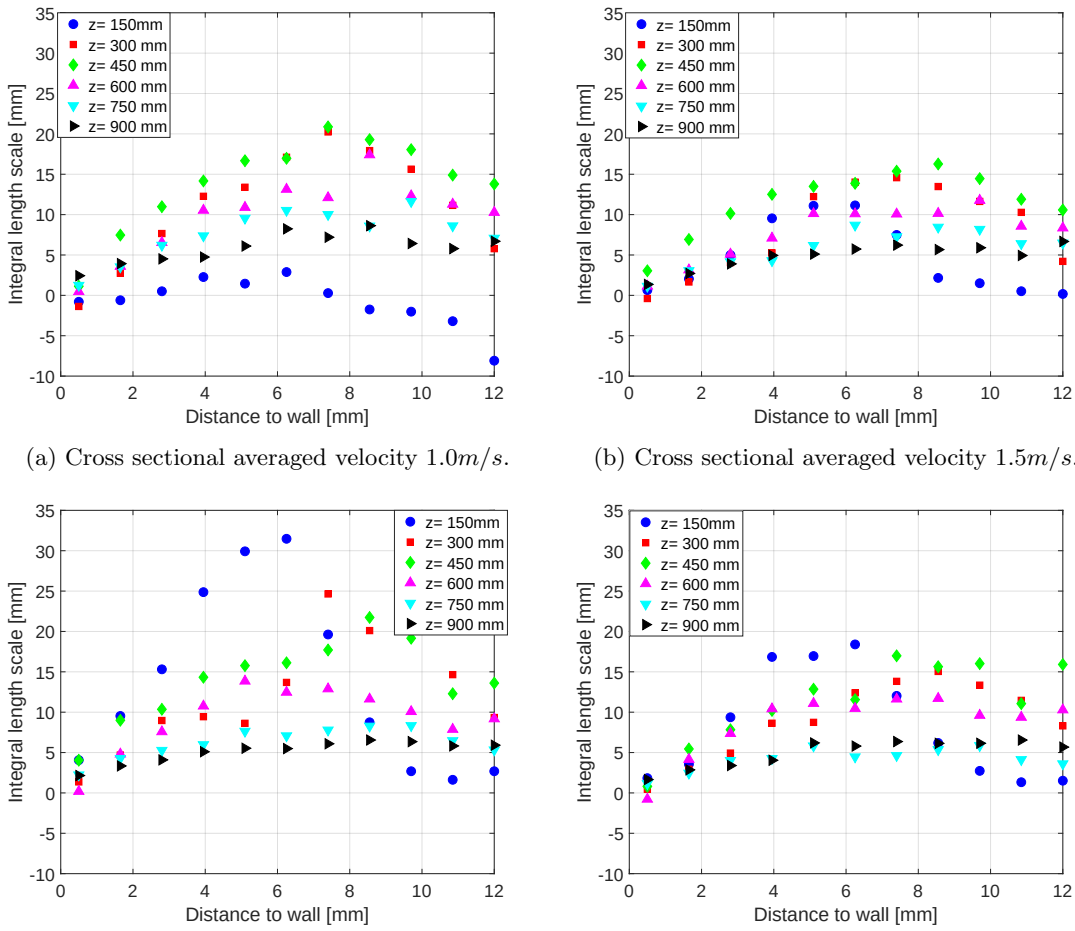

(a) Cross sectional averaged velocity $1.0m/s$.

(b) Cross sectional averaged velocity $1.5m/s$.

(c) Cross sectional averaged velocity $2.0m/s$.

(d) Cross sectional averaged velocity $2.5m/s$.

Figure 6: Integral length scale for different flow conditions. The different measurements correspond to different positions along the channel length.

Since the integral length scale (l) is an estimated parameter, it is of great importance to discuss the error propagation in detail. In particular, the error propagation accounts for the error produced by the integration procedure, in which the values of $Q_{xx}(r)$ were estimated over several measurements, and presents an error estimation for each value of r. The error estimation for the integration of a generic function f can be

expressed as:

$$\delta\left(\int f(x)dx\right) \approx \delta\left(\sum f(x_i)\Delta x_i\right) \tag{44}$$

However, in order to simplify the error estimation, the error for each point will be assumed to be uncorrelated and similar. With these assumptions, the error of the integration can be estimated as:

$$\begin{aligned}\delta\left(\int f(x)dx\right) &\approx \Delta x\sqrt{\sum(\delta f)^2} \\ &\approx \Delta x\sqrt{N_x}\delta f\end{aligned} \tag{45}$$

where Δx is the discretization in the longitudinal direction r, N_x is the amount of integration points and δf is the assumed constant error of the function f at each integration point. Applying this assumptions to the error propagation of Eq. (7) and assuming a limit for the numerical integration at a distance of approximately 10 times the integral length scale, then we obtain the following relation:

$$\frac{\delta\bar{l}}{\bar{l}} = 2\frac{\delta u'_{rms}}{u'_{rms}} + 10\frac{\delta\bar{Q}_{xx}}{u'^2_{rms}\sqrt{N_x}} \tag{46}$$

Here $\bar{Q}_{xx}$ is the constant value used as the estimation of the error of $Q_{xx}(r)$ for the different values of r. The contribution from the velocity fluctuation can be neglected compared to the error contribution from Q_{xx}. The results from applying Eq. (46) can be seen in Fig. 7. It can be observed that the error in the estimation of the integral length scale is considerable.

6. Dissipation rate calculations and error estimation

The dissipation rate can be estimated using different methods as presented in section 2. First, we estimated the turbulent dissipation using the scaling argument presented in Eq. (20). The results from estimating the dissipation rate are presents in Fig. 8, where it can be observed that the dissipation rate is larger closer to the channel wall where the turbulent flow is generated by the structures at the wall, and decreases with the distance to the wall as the turbulent flow propagates through the flow. It can also be observed some increase along the center of the channel (wall distance of $12mm$) as the effects of the entrance effects reduces and the turbulent flow becomes more developed. As expected, it can be observed that the turbulent dissipation rate increase with the mean flow rate.

The error propagation of Eq. 20 results in:

$$\frac{\delta\epsilon}{\epsilon} = 3\frac{\delta u'_{rms}}{u'_{rms}} + \frac{\delta l}{l} \tag{47}$$

The error in the estimation of the velocity fluctuation term is negligible compared with the error in the estimation of the integral length scale. However, as we have acknowledged in section 4.1 the estimation of the velocity fluctuation could be overestimated, and since a power law relates the velocity fluctuation with the turbulent dissipation rate, then we expect the calculation of this to be overestimated close to the channel walls. Fig. 9 shows the error estimated for the turbulent dissipation rate constructed using Eq. (47) for different flow conditions, channel positions and distances to the wall, where it can be observed a larger error closer to the channel walls.

In addition, the scaling argument presents another source of error through the constant parameter A. This parameter value should be in the range $1 - 1.2$. However, many researchers use this as an adjustment parameter and use values outside this range. In this work, the value adopted correspond to $A = 1.1 \pm 0.1$, meaning that the method present an error of 10% given by the range of A.

Another method for obtaining the dissipation rate uses the second order structure function. Considering the turbulent inertial subrange, the dissipation rate can be calculated using the Kolmogorov's two-third law presented in Eq. (10). The approach consists in performing a linear fitting of the second order structure

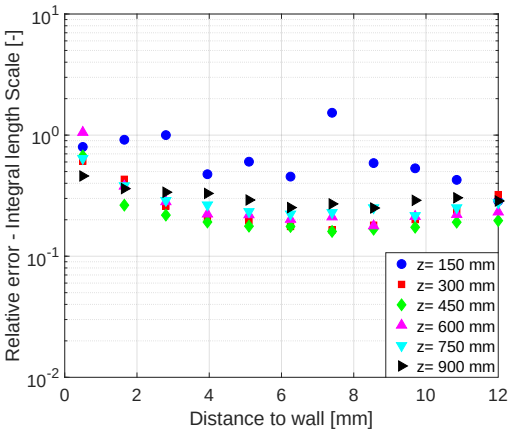

(a) Cross sectional averaged velocity $1.0m/s$.

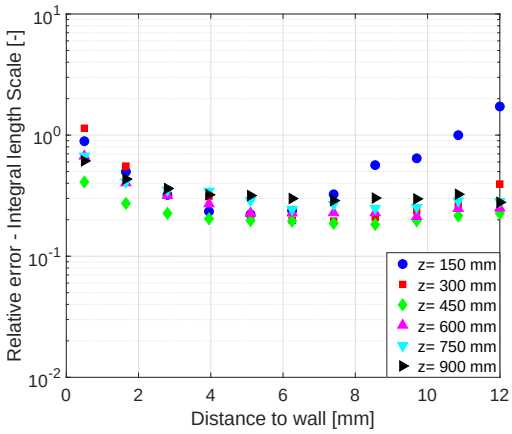

(b) Cross sectional averaged velocity $1.5m/s$.

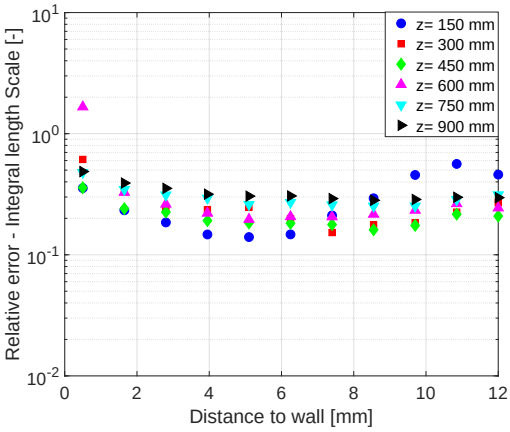

(c) Cross sectional averaged velocity $2.0m/s$.

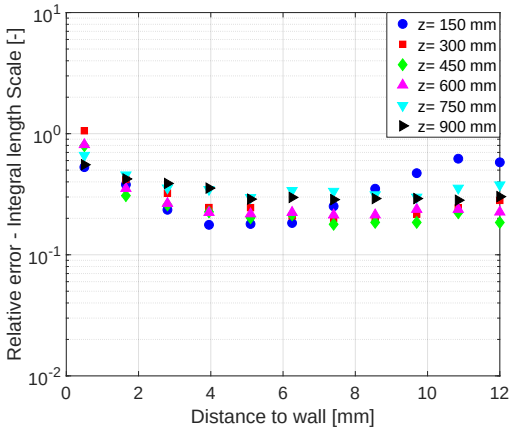

(d) Cross sectional averaged velocity $2.5m/s$.

Figure 7: Estimated error for the integral length scale for different flow conditions. The different measurements correspond to different positions along the channel length.

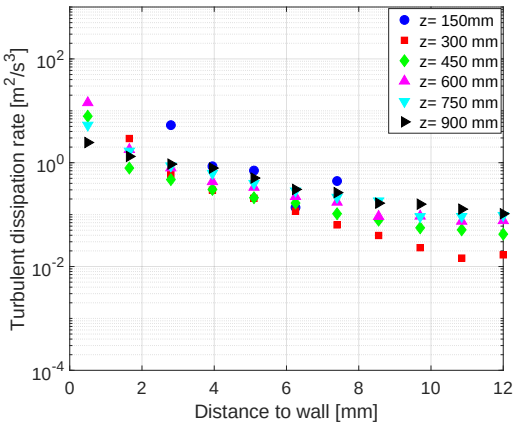

(a) Cross sectional averaged velocity $1.0m/s$.

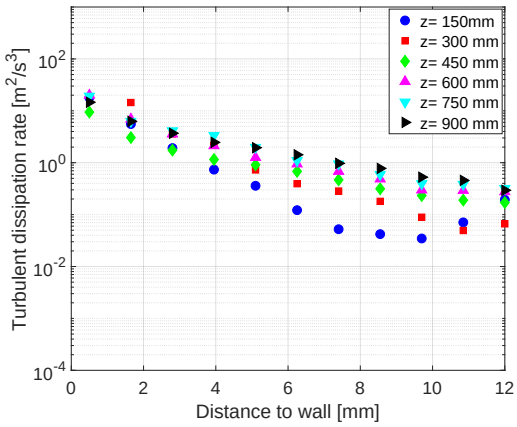

(b) Cross sectional averaged velocity $1.5m/s$.

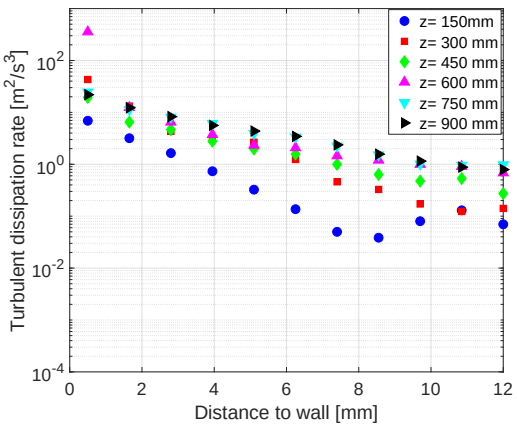

(c) Cross sectional averaged velocity $2.0m/s$.

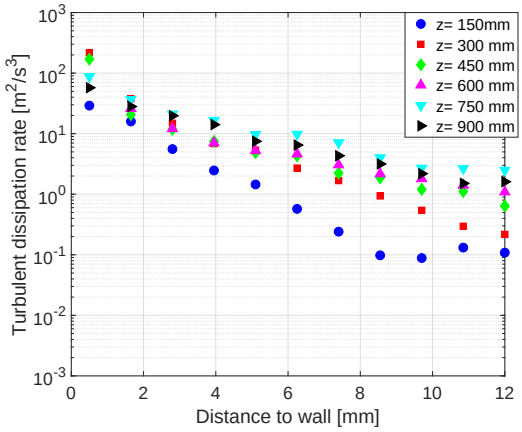

(d) Cross sectional averaged velocity $2.5m/s$.

Figure 8: Dissipation rate estimated using the integral length scale (scaling argument) for different flow conditions. The different measurements correspond to different positions along the channel length.

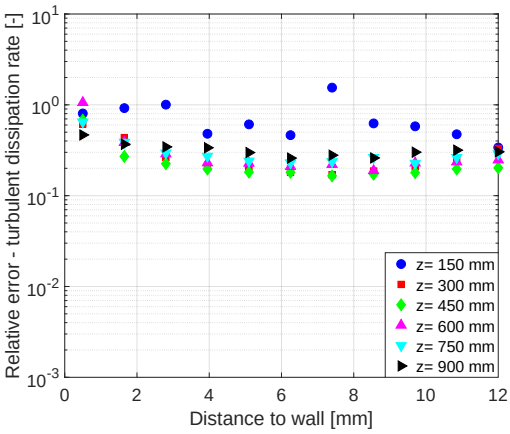

(a) Cross sectional averaged velocity $1.0m/s$.

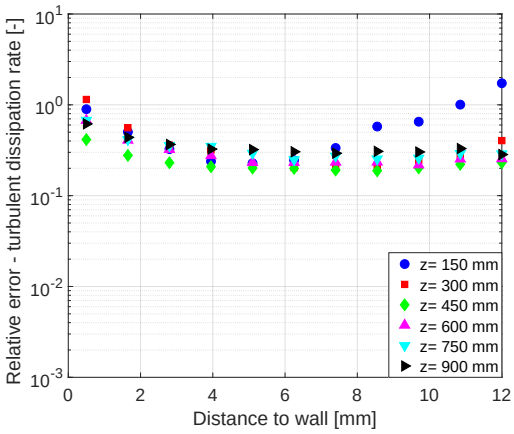

(b) Cross sectional averaged velocity $1.5m/s$.

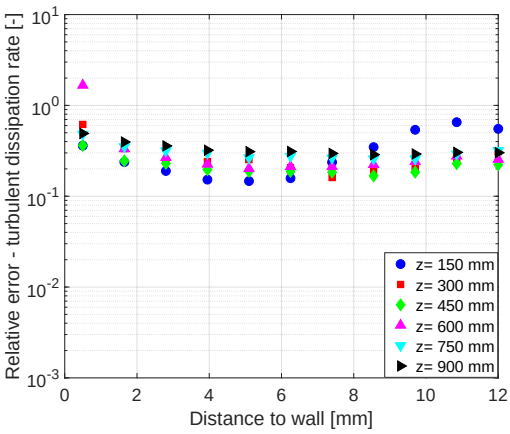

(c) Cross sectional averaged velocity $2.0m/s$.

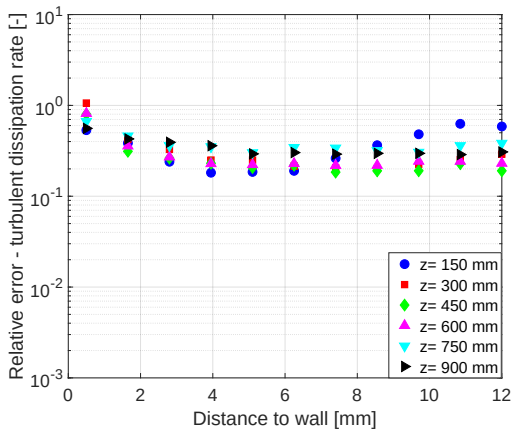

(d) Cross sectional averaged velocity $2.5m/s$.

Figure 9: Estimated error for the dissipation rate calculated using the integral length scale (scaling argument) for different flow conditions. The different measurements correspond to different positions along the channel length.

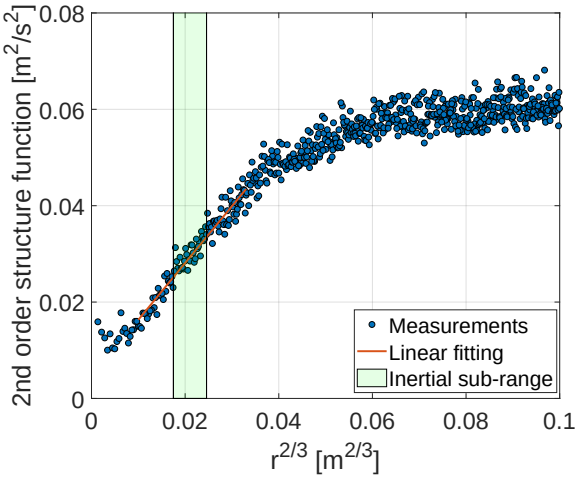

Figure 10: Linear fitting example using the second order structure function in the inertial sub range. The measurement correspond to the center line of the channel at a distance of 600 mm from the channel inlet. The mean cross sectional velocity was 2.0 m/s.

function versus $r^{2/3}$ for the measurement points that correspond to the inertial subrange. The results from the linear fitting provides the value of $\beta\epsilon^{2/3}$, from which the value of the dissipation rate can be easily obtained. An example of this procedure can be seen in Fig. 10, here the measurements were performed at the center line of the channel, from a distance of 600 mm from the inlet of the test section and with a mean cross sectional velocity of 2.0 m/s.

Considered the following a linear representation:

$$y = a + bx \tag{48}$$

Then, using the least squares linear fitting [37], the coefficients a and b can be obtained. In addition, information of the statistical error of the coefficient a and b can be obtained in the form of σ_a and σ_b respectively.

$$a = \frac{\sum x_i^2 \sum y_j - \sum x_i \sum y_j^2}{\Delta} \tag{49}$$

$$b = \frac{N \sum x_i y_i - \sum x_i \sum y_j}{\Delta} \tag{50}$$

$$\Delta = N \sum x_i^2 - (\sum x_i)^2 \tag{51}$$

The error on the coefficient follows:

$$\sigma_y = \sqrt{\frac{1}{N-2}} \sum (y_i - a - bx_i)^2 \tag{52}$$

$$\sigma_a = \sigma_y \sqrt{\frac{\sum x^2}{\Delta}} \tag{53}$$

$$\sigma_b = \sigma_y \sqrt{\frac{N}{\Delta}} \tag{54}$$

Here σ_b reflects the estimated error from the linear fitting from the y coordinate which in this case is the error of $< [\Delta v(r)]^2 >$. Nevertheless, an error was estimated for this quantity since each point is based in an average procedure over several measurements from where a standard deviation was obtained. Then the largest error of these two method were selected. In Fig. 11, the dissipation rate are presented for different

flow conditions and channel positions, where it can be observed that the results obtained with this method are in the same range than the measurements obtained with the scaling argument presented in Fig. 8. Nevertheless, from the comparison between the two methods it can be observe that with this method, the effects of the entrance length are more clearly represented. Here, the turbulent dissipation rate for those positions closer to the entrance presents smaller values close to the middle of the channel (wall distance of $12mm$), and as the distance to the entrance increases, the turbulent dissipation rate converges approximately to the same value.

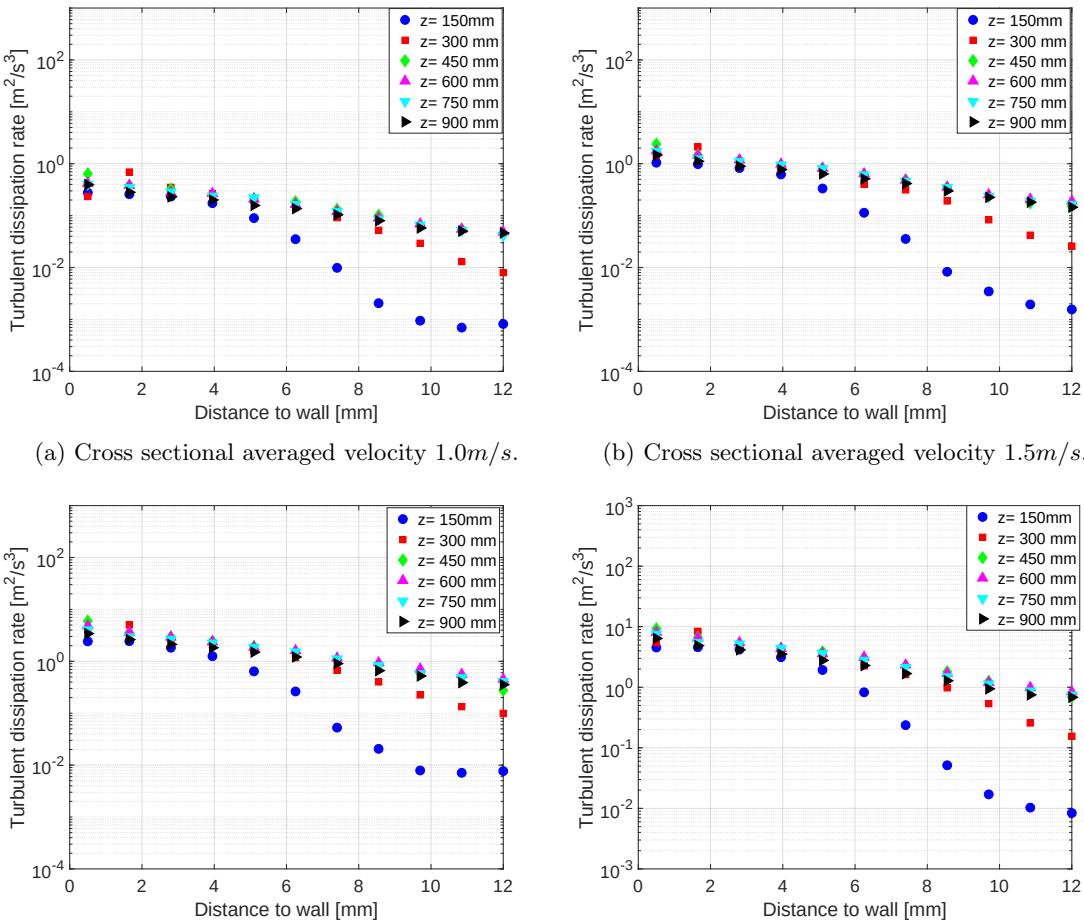

(a) Cross sectional averaged velocity $1.0m/s$.

(b) Cross sectional averaged velocity $1.5m/s$.

(c) Cross sectional averaged velocity $2.0m/s$.

(d) Cross sectional averaged velocity $2.5m/s$.

Figure 11: Dissipation rate estimated using the second order structure function for different flow conditions. The different measurements correspond to different positions along the channel length.

Using the error estimation from the linear fitting presented in Eq. (54), the relative error of the dissipation rate from Eq. (10) follows:

$$\frac{\delta\epsilon}{\epsilon} = \frac{3}{2}\sigma_B \tag{55}$$

The results from applying Eq. (55) can be observed in Fig. 12. It can be observed that with this method the relative error is larger in the center of the channel. This effect is related with the lower turbulence intensities at the middle of the channel that contribute to an increase in the relative error of the turbulent dissipation rate. This effect is more evident for the positions close to the entrance of the channel where the dissipation rate presents lower values. The error produced with this method is considerable smaller than

the error obtained using the integral length scale, due to the error produced in the integration of Q_{xx} which is considerable.

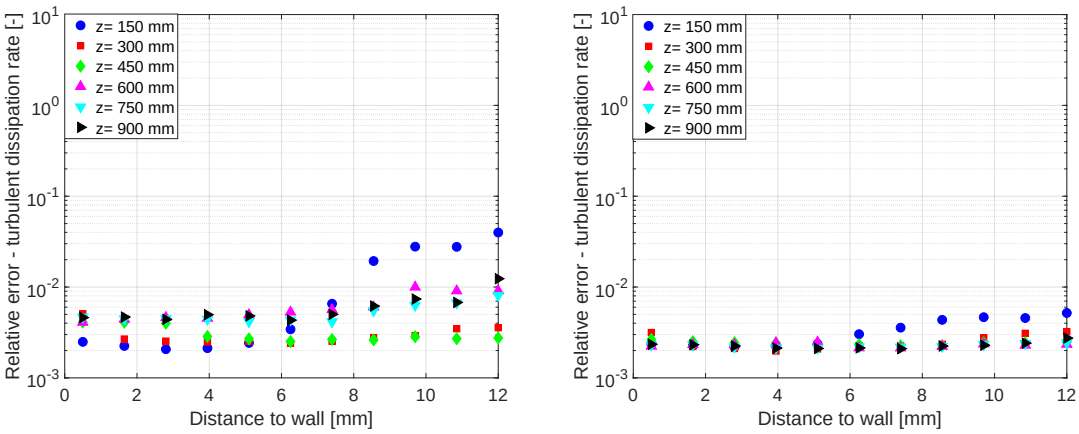

(a) Cross sectional averaged velocity $1.0m/s$.

(b) Cross sectional averaged velocity $1.5m/s$.

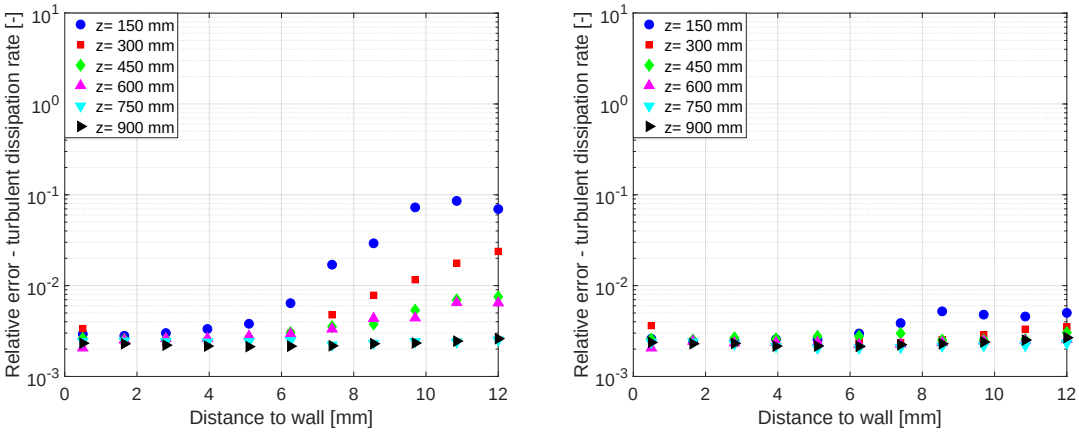

(c) Cross sectional averaged velocity $2.0m/s$.

(d) Cross sectional averaged velocity $2.5m/s$.

Figure 12: Error estimation for the dissipation rate estimated using the second order structure function for different flow conditions. The different measurements correspond to different positions along the channel length.

A similar method consists in using the third order longitudinal structure function, from which the dissipation rate can be obtained through Kolmogorov's four-fifth law presented in Eq. 11. A linear fitting is employed as presented in Eq. 48, in which the parameter y correspond to the third order structure function and the parameter x to the position. An example of fitting the data with this procedure is presented in Fig. 13, where the measurements were performed at the center line of the channel, from a distance of $600\,mm$ from the inlet of the test section and with a mean cross sectional velocity of $2.0\,m/s$. From the linear fitting we obtain the coefficient a, b and σ_a σ_b using the same procedure as with the second order structure function. The dissipation rate obtained are shown in Fig. 14. Here it can be observed the effects of the higher fluctuations of the third order structure function (see Fig. 5) in the estimation of the turbulent dissipation rate. While the values of turbulent dissipation rate obtained are in the same range with the other two methods, it can be clearly see that the results from the second order structure function presents less fluctuation and with a smoother transition between the data generated at different flow conditions and channel position. While this effect can be observed for the different flow condition, it is more evident at lower velocities.

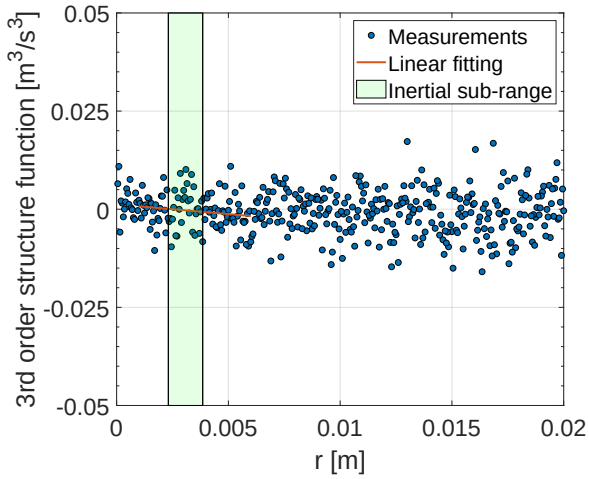

Figure 13: Linear fitting example using the third order structure function in the inertial sub range. The measurement correspond to the center line of the channel at a distance of $600\,mm$ from the channel inlet. The mean cross sectional velocity was $2.0\,m/s$.

Similarly as with previous case, the coefficient σ_b obtained from the linear fitting was compared with the estimated error of the third order structure function and the larger value was then used for estimating the error of the dissipation rate:

$$\frac{\delta\epsilon}{\epsilon} = \frac{5}{4}\sigma_b \tag{56}$$

The estimated error can be seen in Fig. 15. In this case the relative error is larger than using the second order structure function and apparently slightly better that the error from the scaling argument methods. Here the larger fluctuation of the third order structure function contributed to the increase in the error of the estimation of the dissipation rate by mean of the error propagation. This effects is more pronounced at lower velocities and closer to the center of the channel where the turbulent intensity are lower and where it was observed higher fluctuation of the third order structure function presented in Fig. 5.

7. Second order structure function models

In section 2 different methods for turbulent characterization were presented, where the second order structure function was introduced as a mean for obtaining the turbulent dissipation rate. In order to obtain the turbulent dissipation rate the second order structure function was used in the inertial sub range using Kolmogorovs two-third law presented in Eq. 10. Nevertheless, the second order structure function presents information on the entire energy spectrum, which can be used in the development of models for breakage and coalescence that included the contribution from the entire spectrum of turbulence. In Fig. 16, a comparison obtained from measurement of the second order structure function and the models from Solsvik and Jakobsen [9], Gong et. al. [11] and from the numerical integration of Pope's energy spectrum [5] is presented for different flow conditions. The measurement were performed at the centerline of the test section and at a distance of $600\,mm$ from the inlet of the channel. The models were evaluated using the dissipation rate measured using Eq. 10 and using an estimation for the turbulent kinetic energy presented in Eq. 23 based on the measurement of u'_{rms}. With the estimation of k, then integral scale was obtained using Eq. 22. It can be observed that the methods describe fairly well the evolution of the structure function. At higher correlation distances ($r > 20\,mm$), it can be observed that the measurements are better described by Solsvik and Jakobsen model and by the numerical integration of Pope's energy spectrum presented in Eq. 33, with the model of Gong et. al. over predicting the measurements. However, in the inertial sub-range, the model from Gong et. al. and the model from Solsvik and Jakobsen presents similar results which also approximate the measurements better than the numerical integration of the energy spectrum.

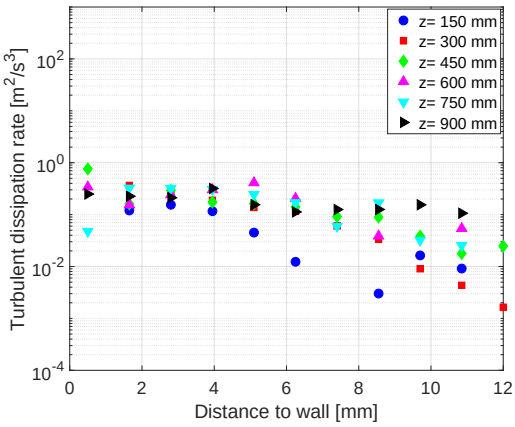

(a) Cross sectional averaged velocity $1.0m/s$.

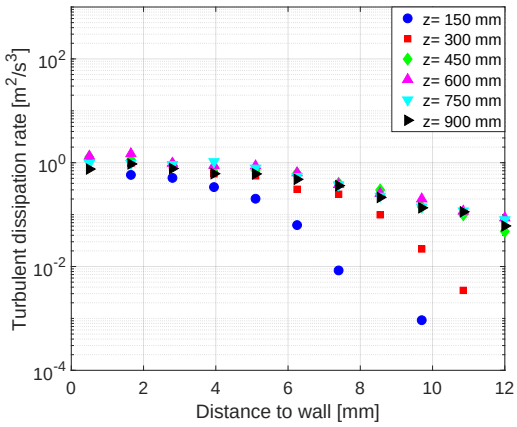

(b) Cross sectional averaged velocity $1.5m/s$.

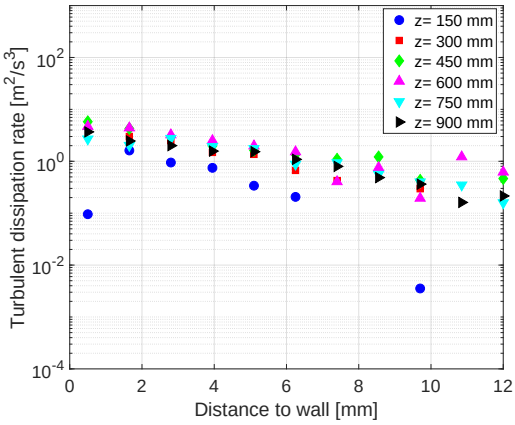

(c) Cross sectional averaged velocity $2.0m/s$.

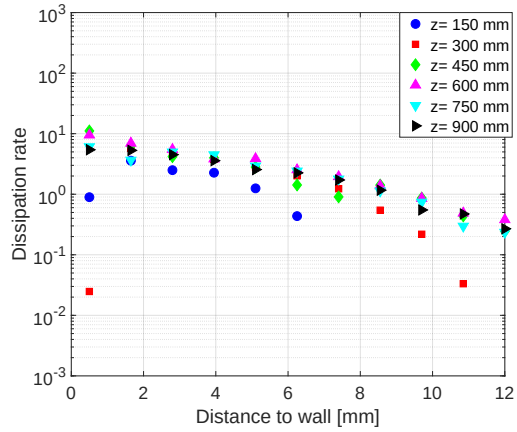

(d) Cross sectional averaged velocity $2.5m/s$.

Figure 14: Dissipation rate estimated using the third order structure function for different flow conditions. The different measurements correspond to different positions along the channel length.

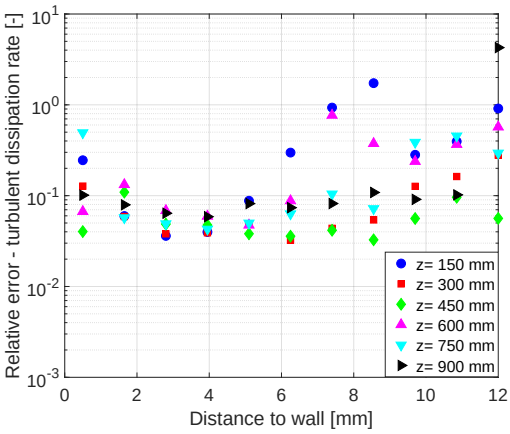

(a) Cross sectional averaged velocity $1.0m/s$.

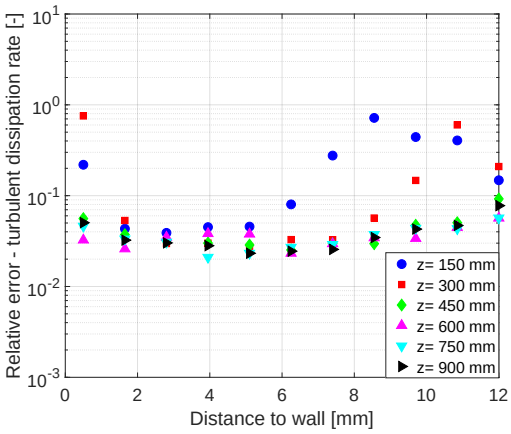

(b) Cross sectional averaged velocity $1.5m/s$.

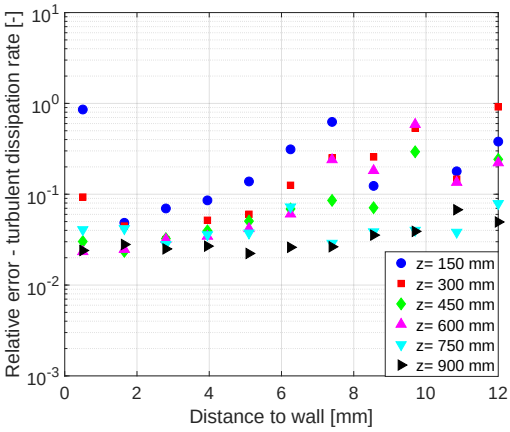

(c) Cross sectional averaged velocity $2.0m/s$.

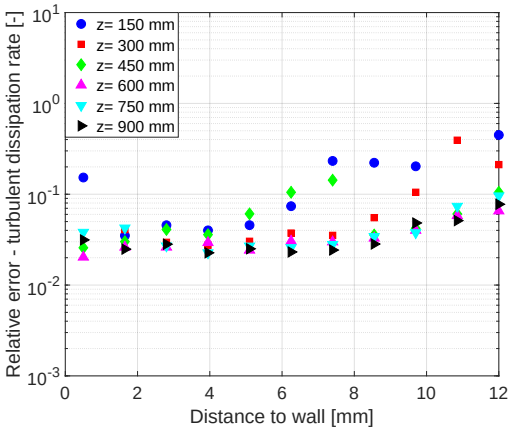

(d) Cross sectional averaged velocity $2.5m/s$.

Figure 15: Error estimation for the dissipation rate determined using the third order structure function for different flow conditions. The different measurements correspond to different positions along the channel length.

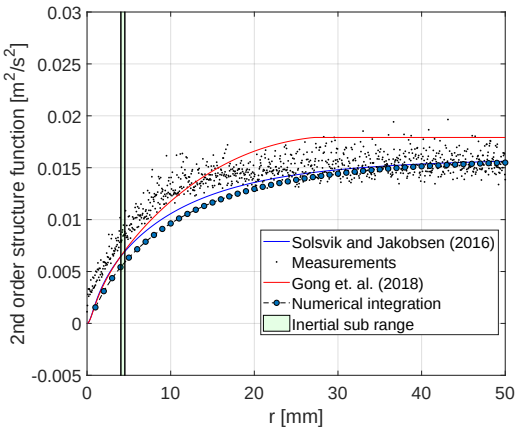

(a) Cross sectional averaged velocity $1.0m/s$.

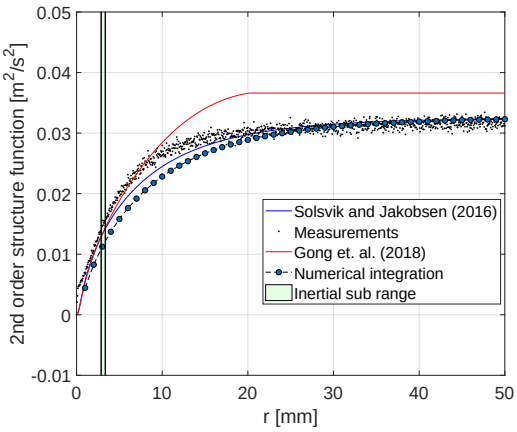

(b) Cross sectional averaged velocity $1.5m/s$.

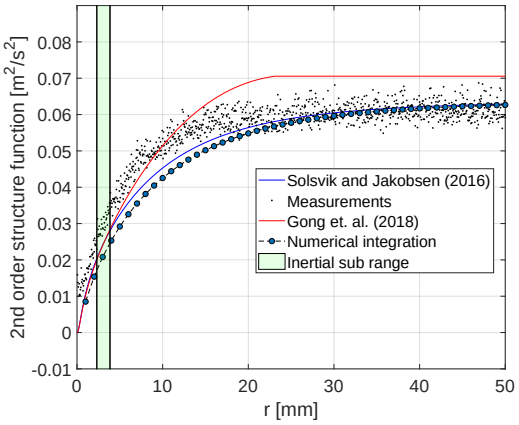

(c) Cross sectional averaged velocity $2.0m/s$.

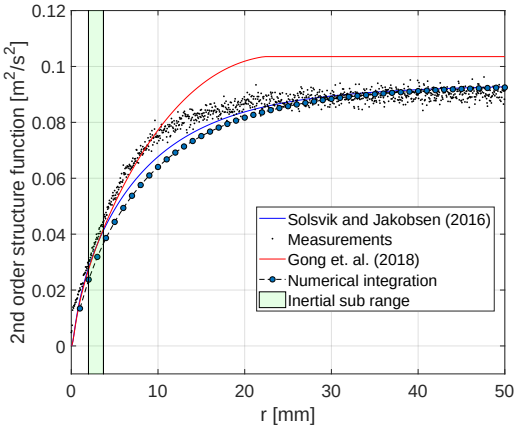

(d) Cross sectional averaged velocity $2.5m/s$.

Figure 16: Second order structure function model comparison at different flow conditions at a distance to the channel inlet of $600\,mm$. The measurement were obtained at the centerline of the channel.

8. Results

In section 4, measurement of the dissipation rate were presented for different methods where the error for each case was discussed. Based on the results obtained, it was found that the estimation of the dissipation rate using the second order structure function presented the smallest uncertainty.

Nevertheless, the other two methods provided results in the same range of values predicting with similar trend the evolution of the turbulent dissipation rate for different wall distance and flow condition. These results are summarized in Fig. 17, where the results from the different methods are presented for different flow conditions and at a distance of 600 mm from the inlet of the channel. Here, the measurement from the different method shows similar results at the middle of the channel. However, closer to the channel wall, the dissipation rate calculated from the scaling argument presented deviation compared to the other two methods which presents similar results in this region. This observation was addressed in section 4.1 where it was discussed that the velocity fluctuation was overestimated close to the channel walls and this is reflected in an overestimation of the dissipation rate using the scaling argument. It can also be observed than the estimations using the third order structure function presents a little more fluctuation than the other two methods, nevertheless it is expected considering the larger uncertainty obtained with this method compared with the second order structure function.

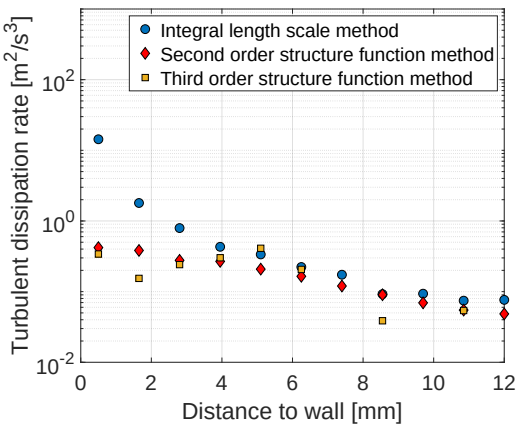

(a) Cross sectional averaged velocity $1.0m/s$.

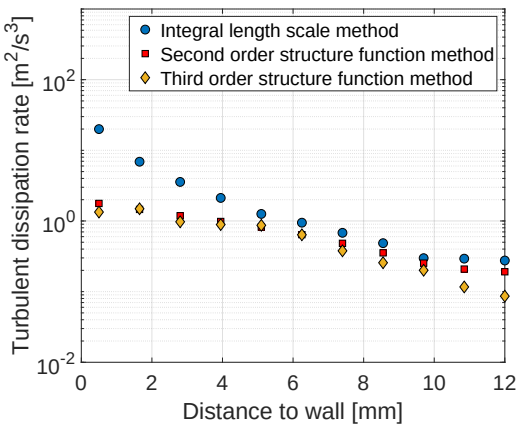

(b) Cross sectional averaged velocity $1.5m/s$.

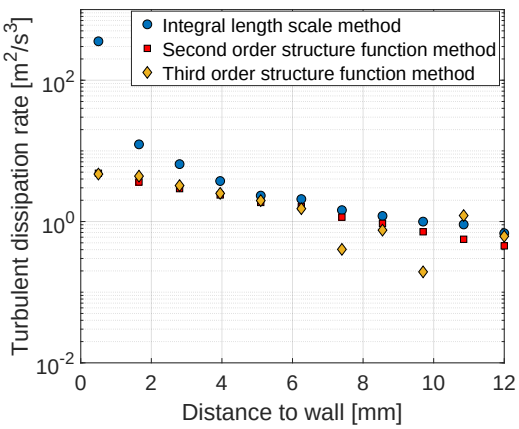

(c) Cross sectional averaged velocity $2.0m/s$.

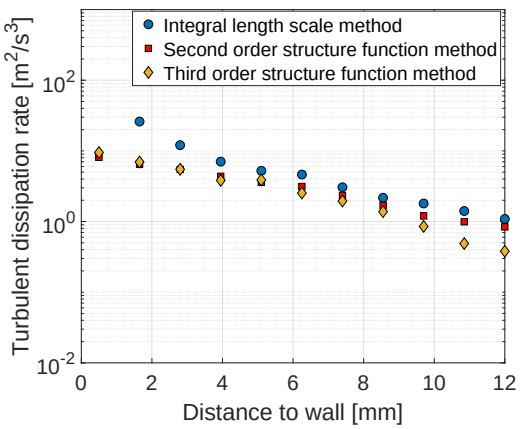

(d) Cross sectional averaged velocity $2.5m/s$.

Figure 17: Comparison of the dissipation rate obtained from the different methods for different flow conditions at a distance of 600 mm from the channel inlet.

Measurement of the turbulent dissipation rate were performed for different positions in the channel and flow conditions. The methods used corresponded to the second order structure function presented in Eq. (10). The methods was chosen due to presenting the best accuracy from the methods reviewed in this work. The results are presented in Fig. 18, where the dissipation rate is presented for different flow conditions and positions in the test section. It can be observed that the dissipation rate intensity is stronger at the channel walls and propagates into the flow as the distance to the inlet of the channel increases.

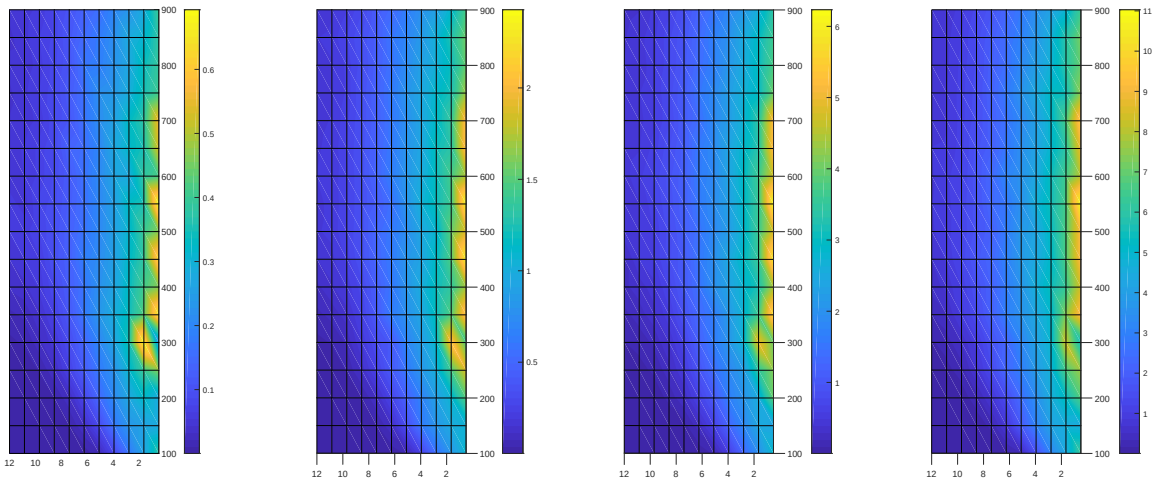

(a) Cross sectional averaged velocity $1.0m/s$.

(b) Cross sectional averaged velocity $1.5m/s$.

(c) Cross sectional averaged velocity $2.0m/s$.

(d) Cross sectional averaged velocity $2.5m/s$.

Figure 18: Dissipation rate estimated using the second order structure function for different flow condition.

The dependence of the dissipation rate with the distance to the channel wall was observed in Fig. 17 where the logarithm of the dissipation rate presented a linear behaviour with the distance to the channel wall. Using these observation, an empirical correlation for the turbulent dissipation rate and the turbulent kinetic energy was found for different flow conditions and distance to the channel walls. The correlation was obtained for the measurement at a distance of $600\,mm$ where we assume a turbulent flow fully developed since the effects that the distance to the channel entrance has on the turbulent dissipation rate can be neglected (see Fig. 18). The correlation obtained follows:

$$\epsilon\left(d_w, Re_d\right) = \exp^{\left(-32.2972-5.42\left[\frac{d_w}{d_h}\right]\right)} Re_d^{3.114} \tag{57}$$

$$k\left(d_w, Re_d\right) = \exp^{\left(-23.1252-3.77\left[\frac{d_w}{d_h}\right]\right)} Re_d^{2} \tag{58}$$

where d_w is the distance from the channel walls, d_h is the hydraulic diameter, and Re_d is the Reynolds number based on the hydraulic diameter:

$$Re_d = \frac{U d_h}{\nu} \tag{59}$$

A comparison between the measured data and the results from the empirical correlation is presented in Fig. 19, where it can be observed that the error of this method is in the range of $\pm 20\%$.

9. Conclusions

We have presented measurements of the turbulent dissipation rate for a rectangular channel using Laser Doppler Velocimetry for direct velocity measurements. The estimation of the dissipation rate presented

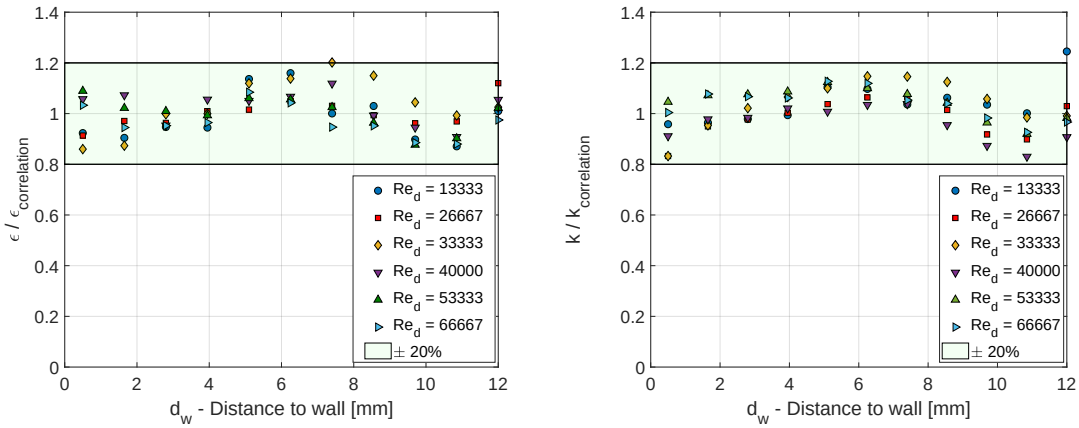

(a) Dissipation rate comparison.

(b) Turbulent kinetic energy comparison.

Figure 19: Comparison between measurements of turbulent dissipation rate and turbulent kinetic energy measurements with estimation using the empirical correlations from Eq. 58.

contains a comparison between the Kolmogorov's two-thirds law, the Kolmogorov's four-fifths law and a scaling argument. We have considered the statistical nature of turbulent flow and performed an uncertainty analysis of each method where we showed the dependence of each method with the measurements statistics. With several available methods for calculating the dissipation rate, it is important to note the uncertainty in the value presented, such that later modeling attempts may treat the information correctly.

The methods for estimating the turbulent dissipation rate are statistical methods that required the use of two-points correlations. These were obtained by using direct velocity measurement with the LDV and by applying the Taylor's frozen hypothesis for transforming a time dependent velocity into a spatial velocity field required for the calculation of two-point correlation. The two point correlation used were the velocity autocorrelation function, the second order structure function and the third order structure function.

We observed that the methods presented in this work showed similar results and trends with respect to changes in flow condition and distance to the channel walls. It was also observed that a significant larger increase in the estimated turbulent dissipation rate was observed close to the channel wall in the scaling argument method compared to the other methods. However, the deviation in this estimation could be explained by acknowledging the uncertainty of the velocity fluctuation measurements close to the channel wall, which greatly affects the estimation of the scaling argument. The comparison between the uncertainties in the estimation for each method also showed that by using the Kolmogorov's two-thirds law a smaller statistical uncertainty was achieved.

The measurement of the second order structure function were compared with the models from Solsvik and Jakobsen [9] and Gong et. al. [11]. The relevance of these two models is founded in the possibility of implementing breakage and coalescence models for the entire energy spectrum. The results from the comparison showed a good agreement with both methods for the inertial and energy containing sub-range. The acurracy required for the comparison between measurement of the second order structure function and the models from Solsvik and Jakobsen [9] and Gong et. al. [11] for the dissipation sub-range was not achieved, and as a consequence the validity of this two models in this sub-range were not discussed in this work.

Finally, an empirical correlation for the dissipation rate for fully developed turbulent flow was presented. A comparison between measurement and the empirical correlation presented an estimated error in the range of ±20%.

10. Acknowledgement

This work was carried out as a part of SUBPRO, a Research-based Innovation Centre within Subsea Production and Processing. The authors gratefully acknowledge the financial support from SUBPRO, which is financed by the Research Council of Norway, major industry partners and NTNU.

Appendix A. Complementary measurements

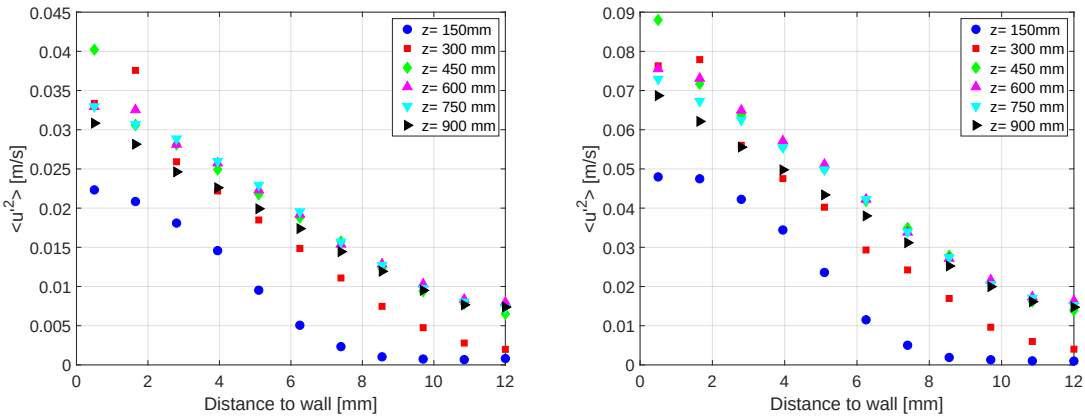

(a) Mean velocity $1.0m/s$.

(b) Mean velocity $1.5m/s$.

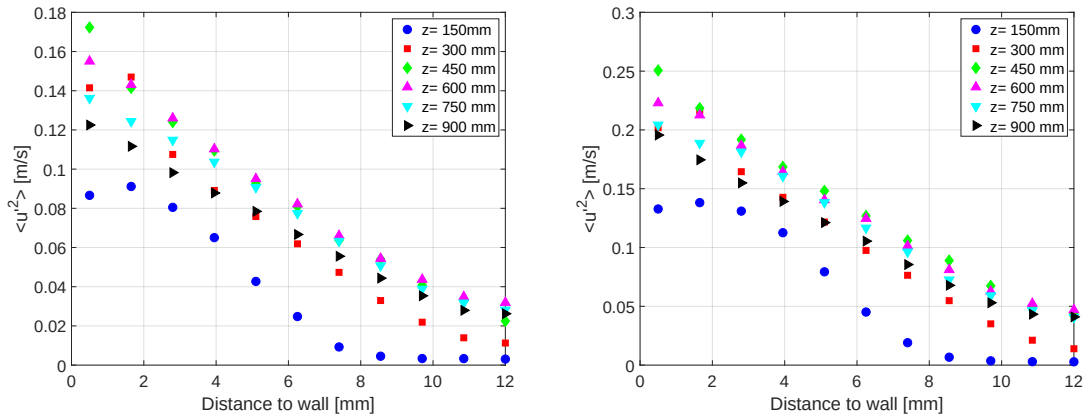

(c) Mean velocity $2.0m/s$.

(d) Mean velocity $2.5m/s$.

Figure A.20: Velocity fluctuations for different flow conditions. The different measurements correspond to different positions along the channel length.

References

[1] T. Lemenand, P. Dupont, D. Della Valle, H. Peerhossaini, Comparative efficiency of shear, elongation and turbulent droplet breakup mechanisms: Review and application, Chemical Engineering Research and Design 91 (2013) 2587–2600.

[2] C. Coulaloglou, L. Tavlarides, Drop size distributions and coalescence frequencies of liquid-liquid dispersions in flow vessels, American Institute of Chemical Engineers journal 22 (2) (1976) 289–297.

[3] F. Azizi, A. Al Taweel, Turbulently flowing liquid-liquid dispersions. part i: drop breakage and coalescence, Chemical Engineering Journal 166 (2) (2011) 715–725.

[4] L. Han, S. Gong, Y. Li, N. Gao, J. Fu, H. A. Luo, Z. Liu, Influence of energy spectrum distribution on drop breakage in turbulent flows, Chemical Engineering Science 117 (2014) 55–70.
[5] S. B. Pope, Turbulent Flows, Cambridge University Press, 2000.
[6] J. O. Hinze, Turbulence, McGraw-Hill, NewYork, 1975.
[7] R. Andersson, B. Andersson, Modelling the breakup of fluid particles in turbulent flows, American Institute of Chemical Engineers Journal 52 (2006) 2031–2038.
[8] S. Maaß, M. Kraume, Determination of breakage rates using single drop experiments, Chemical Engineering Science 70 (2012) 146–164.
[9] J. Solsvik, H. A. Jakobsen, Development of fluid particle breakup and coalescence closure models for the complete energy spectrum of isotropic turbulence, Industrial & Engineering Chemistry Research 55 (5) (2016) 1449–1460.
[10] J. Solsvik, H. A. Jakobsen, A review of the statistical turbulence theory required extending the population balance closure models to the entire spectrum of turbulence, American Institute of Chemical Engineers journal.
[11] S. Gong, L. Han, H. Luo, A novel multiscale theoretical model for droplet coalescence induced by turbulence in the framework of entire energy spectrum, Chemical Engineering Science 176 (2018) 377–399.
[12] P. A. Davidson, Turbulence: An Introduction for Scientists and Engineers, 2ed., Oxford University Press, 2015.
[13] G. I. Taylor, The spectrum of turbulence, Proceedings of the Royal Society of London. Series A, Mathematical and Physical Sciences 164 (919) (1938) 476–490.
[14] M. Bouaifi, M. Mortensen, R. Andersson, W. Orciuch, B. Andersson, F. Chopard, T. Noren, Experimental and numerical investigation of a jet mixing in a multifunctional channel reactor. passive and reactive system, Chemical Engineering Research and Design 82 (2004) 274–283.
[15] R. Andersson, B. Andersson, F. Chopard, T. Noren, Development of a multi-scale simulation method for design of novel multiphase reactors, Chemical Engineering Science 59 (2004) 4911–4917.
[16] R. Andersson, B. Andersson, On the breakup of fluid particles in turbulent flows, American Institute of Chemical Engineers Journal 52 (2006) 2020–2030.
[17] S. Maaß, A. Gabler, A. Zaccone, A. Paschedag, M. Kraume, Experimental investigations and modelling of breakage phenomena in stirred liquid/liquid systems, Chemical Engineering Research and Design 85 (2012) 703–709.
[18] S. Maaß, F. Metz, T. Rehm, M. Kraume, Prediction of drop sizes for liquid-liquid systems in stirred slim reactors - part i: Single stage impellers, Chemical Engineering Journal 162 (2010) 792–801.
[19] S. Maaß, N. Paul, M. Kraume, Influence of the dispersed phase fraction on experimental and predicted drop size distribution in breakage dominated stirred systems, Chemical Engineering Science 76 (2012) 140–153.
[20] A. Håkansson, H. H. Mortensen, R. Andersson, F. Innings, Experimental investigation of turbulent fragmenting stresses in a rotor-stator mixer. par 1. estimation of turbulent stresses and comparison to breakup visualizations, Chemical Engineering Science 171 (2017) 625–637.
[21] H. H. Mortensen, F. Innings, A. Håkansson, Local levels of dissipation rate of tubulent kinetic energy in a rotor-stator mixer with different stator slot widths - an experimental investigation, Chemical Engineering Research and Design 130 (2018) 52–62.
[22] J. de Jong, L. Cao, S. Woodward, J. Salazar, L. Collins, H. Meng, Dissipation rate estimation from piv in zero-mean isotropic turbulence, Experiments in fluids 46 (3) (2009) 499–515.
[23] J. Sheng, H. Meng, R. O. Fox, A large eddy piv method for turbulence dissipation rate estimation, Chemical Engineering Science 55 (2000) 4423–4434.
[24] J. Smagorinsky, General circulation experiments with the primitive equations: 1. the basic experiment, Monthly Weather Review 91 (3) (1963) 99–162.
[25] J. Vejražka, M. Zedníková, P. Stanovský, Experiments on breakup of bubbles in a turbulent flow, American Institute of Chemical Engineers Journal 0 (0).
[26] T. Lemenand, D. Della Valle, C. Habchi, H. Peerhossaini, Micro-mixing measurement by chemical probe in homogeneous and isotropic turbulence, Chemical Engineering Journal 314 (2017) 453–465.
[27] T. Lemenand, D. Della Valle, P. Dupont, H. Peerhossaini, Turbulent spectrum model for drop-breakup mechanisms in an inhomogeneous turbulent flow, Chemical Engineering Science 158 (2017) 41–49.
[28] A. N. Kolmogorov, The local structure of turbulence in incompressible viscous fluid for very large reynolds numbers, Dokl. Akad. Nauk SSSR 30 (4) (1941) 299–303. [English translation in Proc R Soc London Ser A 434:9–13 (1991)].
[29] J. Shi, E. H. Herø, J. Solsvik, H. A. Jakobsen, Experimental and numerical study on single droplet breakage in turbulent flow, 12th International Conference on CFD in Oil & Gas, Metallurgical and Process Industries.
[30] E. H. Herø, N. La Forgia, J. Shi, J. Solsvik, H. A. Jakobsen, On the turbulent dissipation rate in experimental investigation of single droplet breakage in fluid-liquid system, PBE 2018 conference.
[31] A. N. Kolmogorov, A refinement of previous hypotheses concerning the local structure of turbulence in a viscous incompressible fluid at high reynolds number, Journal of Fluid Mechanics 13 (1962) 82–85.
[32] G. I. Taylor, Statistical theory of turbulence. i, Proceedings of the Royal Society A 151 (873) (1935) 421–444.
[33] H. Tennekes, J. L. Lumley, A First Course in Turbulence, The MIT Press, 1972.
[34] J. Solsvik, Turbulence modeling in the wide energy spectrum: Explicit formulas for reynolds number dependent energy spectrum parameters, European Journal of Mechanics-B/Fluids 61 (2017) 170–176.
[35] B. Sawford, J. Hunt, Effects of turbulence structure, molecular diffusion and source size on scalar fluctuations in homogeneous turbulence, Journal of Fluid Mechanics 165 (1986) 373–400.
[36] V. A. Iyer, M. A. Woodmansee, Uncertainty analysis of laser-doppler-velocimetry measurements in a swirling flowfield, American Institute of Aeronautics and Astronautics Journal 43 (3) (2005) 512–519.
[37] J. R. Taylor, An introduction to error analysis, second edition, University Science Books, 1997.